NAVAL POSTGRADUATE SCHOOL
MONTEREY, CALIFORNIA

THESIS

BOUNDARY CURVATURE EFFECTS ON GAS BUBBLE OSCILLATIONS IN UNDERWATER EXPLOSION

by

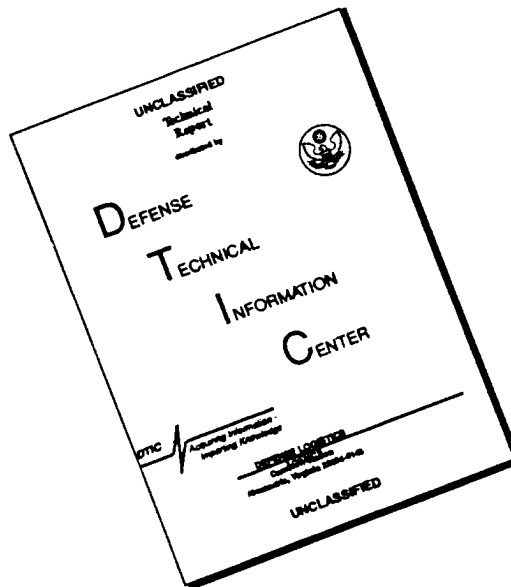Kazuhiro Matsumoto

March 1996

Thesis Advisor: Young S. Shin

Approved for public release; distribution is unlimited.

DTIC QUALITY INSPECTED 1

DISCLAIMER NOTICE

THIS DOCUMENT IS BEST QUALITY AVAILABLE. THE COPY FURNISHED TO DTIC CONTAINED A SIGNIFICANT NUMBER OF PAGES WHICH DO NOT REPRODUCE LEGIBLY.

REPORT DOCUMENTATION PAGE

Form Approved OMB No. 0704-0188

1. AGENCY USE ONLY *(Leave blank)*	2. REPORT DATE March 1996	3. REPORT TYPE AND DATES COVERED Master's Thesis

4. TITLE AND SUBTITLE BOUNDARY CURVATURE EFFECTS ON GAS BUBBLE OSCILLATIONS IN UNDERWATER EXPLOSION	5. FUNDING NUMBERS
6. AUTHOR(S): Kazuhiro Matsumoto	

7. PERFORMING ORGANIZATION NAME(S) AND ADDRESS(ES) Naval Postgraduate School Monterey, CA 93943-5000	8. PERFORMING ORGANIZATION REPORT NUMBER

9. SPONSORING/MONITORING AGENCY NAME(S) AND ADDRESS(ES)	10. SPONSORING/MONITORING AGENCY REPORT NUMBER

11. SUPPLEMENTARY NOTES The views expressed in this thesis are those of the author and do not reflect the official policy or position of the Department of Defense or the U.S. Government.

12a. DISTRIBUTION/AVAILABILITY STATEMENT Approved for public release; distribution is unlimited.	12b. DISTRIBUTION CODE

13. ABSTRACT *(maximum 200 words)*

The oscillation of a gas bubble produced as a result of underwater explosion could cause the severe whipping damage on nearby marine vehicle. The effects of rigid boundary curvatures to explosive gas bubble oscillation behavior in underwater were investigated. The analyses were conducted using a multimaterial Lagrangian-Eulerian finite element code, MSC/DYTRAN. The incident shock wave pressure, bubble pulse pressure, gas bubble radius and period were calculated for the case of detonation of a charge near the curved rigid boundary. The results were compared for the case of free field bubble oscillations.

14. SUBJECT TERMS Underwater Explosion, Boundary Condition, Bubble			15. NUMBER OF PAGES 72
			16. PRICE CODE

17. SECURITY CLASSIFICATION OF REPORT Unclassified	18. SECURITY CLASSIFICATION OF THIS PAGE Unclassified	19. SECURITY CLASSIFICATION OF ABSTRACT Unclassified	20. LIMITATION OF ABSTRACT UL

NSN 7540-01-280-5500 Standard Form 298 (Rev. 2-89)
Prescribed by ANSI Std. 239-18 298-102

BOUNDARY CURVATURE EFFECTS ON GAS BUBBLE OSCILLATIONS IN UNDERWATER EXPLOSION

Kazuhiro Matsumoto
Lieutenant, Japanese Maritime Self Defense Force
B.S., The Technological University of Nagaoka, 1986
M.S., The Technological University of Nagaoka, 1988
Submitted in partial fulfillment
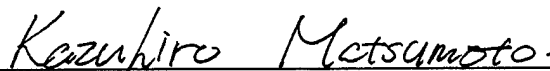of the requirements for the degree of

MASTER OF SCIENCE IN MECHANICAL ENGINEERING

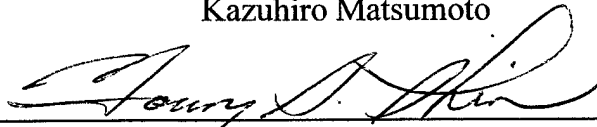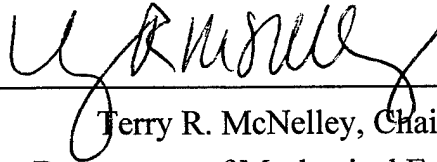from the

NAVAL POSTGRADUATE SCHOOL
March 1996

Author: _____

Kazuhiro Matsumoto

Approved by: _____

Young S. Shin, Thesis Advisor

_____

Terry R. McNelley, Chairman
Department of Mechanical Engineering

iv

ABSTRACT

The oscillation of a gas bubble produced as a result of underwater explosion could cause the severe whipping damage on nearby marine vehicle. The effects of rigid boundary curvatures to explosion gas bubble oscillation behavior in underwater were investigated. The analyses were conducted using a multimaterial Lagrangian-Eulerian finite element code, MSC/DYTRAN. The incident shock wave pressure, bubble pulse pressure, gas bubble radius and period were calculated for the case of detonation of a charge near the curved rigid boundary. The results were compared for the case of free field bubble oscillations.

TABLE OF CONTENTS

LIST OF FIGURES

LIST OF TABLES

ACKNOWLEDGMENT

I. INTRODUCTION

When a charge detonates in underwater, it emits energy to the surrounding water and converts the original material into a gas sphere (called the bubble) at very high temperature and pressure. The emitted energy, which has about half of the energy of the explosion, appears as a shock wave. During the transmission of the shock wave to the surrounding fluid, the initial high pressure in the gas sphere is considerably decreased, but it is still much higher than the surrounding pressure, which is atmospheric plus hydrostatic pressure. As the shock wave passes each water particle, the water particle attains a radial velocity. This motion of the water particle behind the shock wave front is essentially incompressible flow after the pressure in the water drops to near hydrostatic pressure. Thus it is reasonable to use incompressible flow theory to describe the bubbles motion and behavior. Initially, the bubble has a large outward velocity and its diameter increases rapidly. The expansion continues for a relatively long time, and the internal bubble pressure decreases gradually, but the motion persists because of the inertia of the outward flowing water. At a later time, the pressure in the bubble falls below the equilibrium value determined by the surrounding pressure and the pressure defect brings the outward flow to stop and the bubble begins to contract at an increasing rate. As bubble approaches minimum radius, the bubble produces a pressure pulse, called the bubble pulse. The bubble pulse can give a radial velocity to water particle and cause damage just as the initial shock

wave can. The bubble contains about half of the total explosion energy[Ref. 1]. Explosions in air emits a shock wave which has the most of explosion energy, and do not form a bubble like an underwater explosion. In underwater explosion analysis, the bubble can be as important as the initial shock wave.

Explosive gas bubble behavior in the free field case and several simple boundary cases was studied by Chisum[Ref.2]. The effects of rigid boundary curvatures on gas bubble oscillation behavior in underwater explosions was investigated. The analyses were conducted using the multimaterial Lagrangian-Eulerian finite element code MSC/DYTRAN. The incident shock wave pressure, bubble pulse pressure, gas bubble radius and period were calculated for the detonation of a charge near various curved rigid boundaries. The results were compared with the free field bubble oscillation.

II. NUMERICAL COMPUTER CODE

In this study, the materials analyzed are fluids (gas and seawater). The Eulerian finite element technique, which is frequently used for analyses of fluids or materials that undergo very large deformations, and in which the grid points are fixed in space and the material moves through the Eulerian mesh (see Figure 1) is used. The mass, momentum and energy of the material are transported from element to element. The Eulerian method calculates the motion of material through elements of constant volume with respect to time(see Figure 2). MSC/DYTRAN is capable of finite element analyses using to 9 Eulerian materials. In the MSC/DYTRAN code, the Eulerian mesh is defined in exactly the same manner as a Lagrangian mesh. General connectivity is used, so the Eulerian mesh can be of an arbitrary shape and have an arbitrary numbering system. This offers considerably more flexibility than the logical rectangular meshes used in other Eulerian codes. However, the use of an Eulerian mesh is different from that of the Lagrangian type. The most important aspect of modeling with the Eulerian technique is that the mesh must be large enough to contain the material after deformation. A basic Eulerian mesh acts like a container and, unless specifically defined, material cannot leave the mesh. Stress wave reflections and pressure built-up can develop from an Eulerian mesh that is too small for the analysis.

Figure 1.   Transportation of Mass, Momentum and Energy through Eulerian Elements
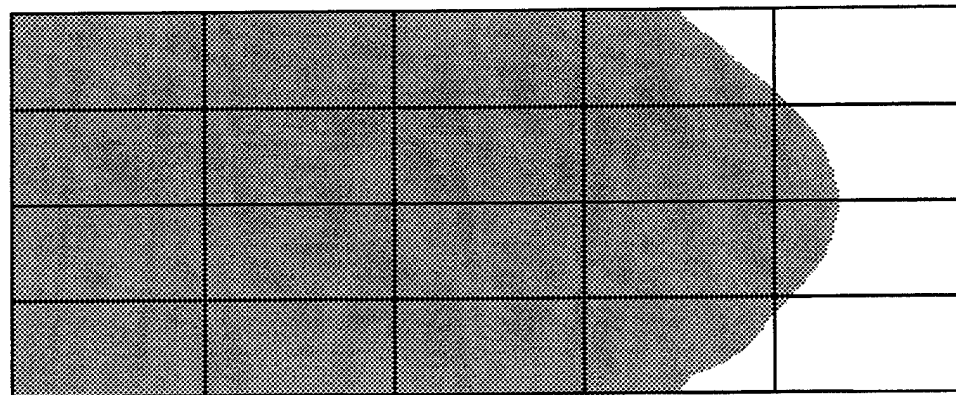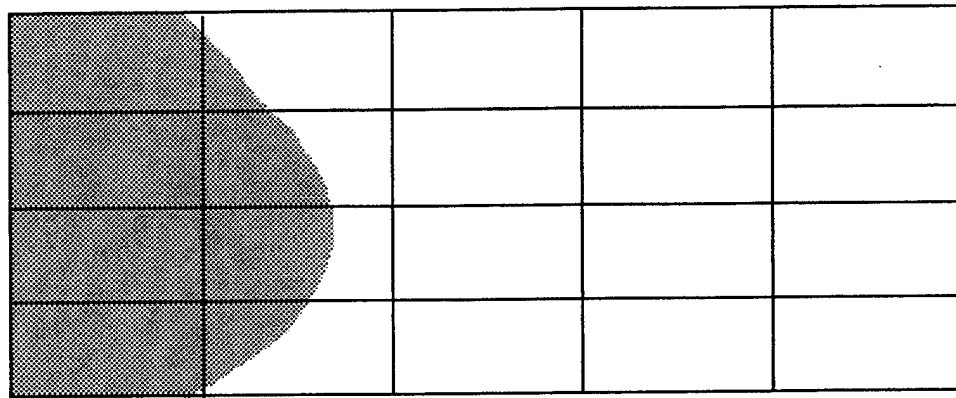
Figure 2. Motion of Material through Eulerian Elements

III. MODELING AND SIMULATION

In order to investigate the effects of rigid boundary curvature on explosion gas bubble behavior, the free field case which has no boundary was analyzed first, to provide basic information about the bubble. Cases in which the explosion takes place near a flat rigid boundary were then simulated, to compare to cases with curved rigid boundaries. Finally, curved rigid boundary cases were analyzed. In this study, the charge modeled is a 10.24kg cylinder of TNT, 20cm in a diameter and 20cm height, submerged in a seawater at a depth of 1000m. The TNT was modeled using a Jones-Wilkins-Lee (JWL) equation of state, with standard equations and parameters for TNT [Ref. 4]. With this equation, the pressure in the "burned fraction" of the explosive material is related to the specific internal energy and density by :

$$p = A(1 - \frac{\omega\eta}{R_1})e^{-\frac{R_1}{\eta}} + B(1 - \frac{\omega\eta}{R_2})e^{-\frac{R_2}{\eta}} + \omega\eta\rho_0 E \qquad (1)$$

where $\eta = \rho/\rho_0$

ρ_0 = initial density

E = specific internal energy (per unit mass)

A, B, ω, R_1, R_2 are constants for the explosive

The explosive was modeled as a homogeneous mass of TNT. The equation of state parameters used were :

$$\rho_0 = 1630 \text{ kg}/\text{m}^3$$

$$E = 20076 \text{ J}/\text{kg}$$

$$A = 3.712 \times 10^{11} \text{ Pa}$$

$$B = 3.231 \times 10^9 \text{ Pa}$$

$$\omega = 0.30$$

$$R_1 = 4.15$$

$$R_2 = 0.95$$

$$d = 6390 \text{ m}/\text{s}$$

In order to model the seawater in which the explosion occurs, a polynomial equation of state was used. This state of equation relates the pressure in the fluid to the acoustic condensation μ and the specific internal energy by;

$$p = a_1\mu + a_2\mu^2 + a_3\mu^3 + (b_0 + b_1\mu + b_2\mu^2)\rho_0 E \qquad (\mu > 0)$$

$$\qquad (2)$$

$$p = a_1\mu + (b_0 + b_1\mu)\rho_0 E \qquad (\mu < 0)$$

where $\qquad \mu = (\rho - \rho_0)/\rho_0$

ρ_0 = initial density

E = specific internal energy (per unit mass)

$a_0, a_1, a_2, b_0, b_1, b_2$ are constants for the fluid

and the upper equation applies to a fluid in a compressed state, while the lower applies to a fluid in a expanded state. Constants were determined by Chisum [Ref. 2].

A. FREE FIELD CASE

The free field case was investigated first. As deep submerged charges are known to undergo little vertical migration due to gravity [Ref. 1], a quasi one dimensional finite

element model, in which gravity is neglected entirely, was used for this analysis. The problem thus has spherical symmetry. The geometry of this problem is shown in Figure 3.

p (atm) = 0.1013 MPa

y=1000m   distance r = 0.71m

p (atm) = 0.1013 MPa

$\rho = 1025 \ kg/m^3$

$g = 9.80665 \ m/s^2 \ (\downarrow)$

$p_\infty = p(atm) + \rho g y$

$(= 10.15 MPa)$

charge (10.24kg TNT)   pressure measure point (r : standoff distance)
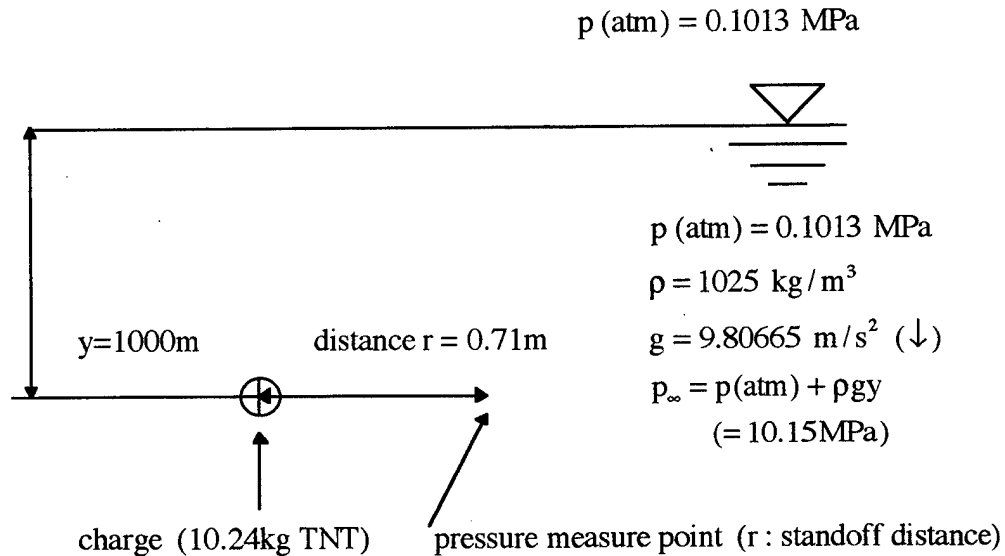
Figure 3.   Deep Spherical Bubble Problem Geometry

The overall geometry of the finite element model for this quarter symmetry axisymmetric free field analysis is shown in Figure 4, from a three dimensional perspective. Figure 5 shows the complete finite element model for this analysis from a two dimensional perspective. The distance of 400m from the charge to the boundary was chosen because at this distance, reflected wave form the boundary did not affect the results during this analysis. A close up view of the lower right corner of Figure 5, which includes the "central" which was a refined region near the charge and "transition" region which was used to connect the central and outside regions, and a small portion of the "outside" region which can be thought of as "storing" energy and momentum during bubble expansion, which then effects bubble collapse after the momentum field reverses direction,
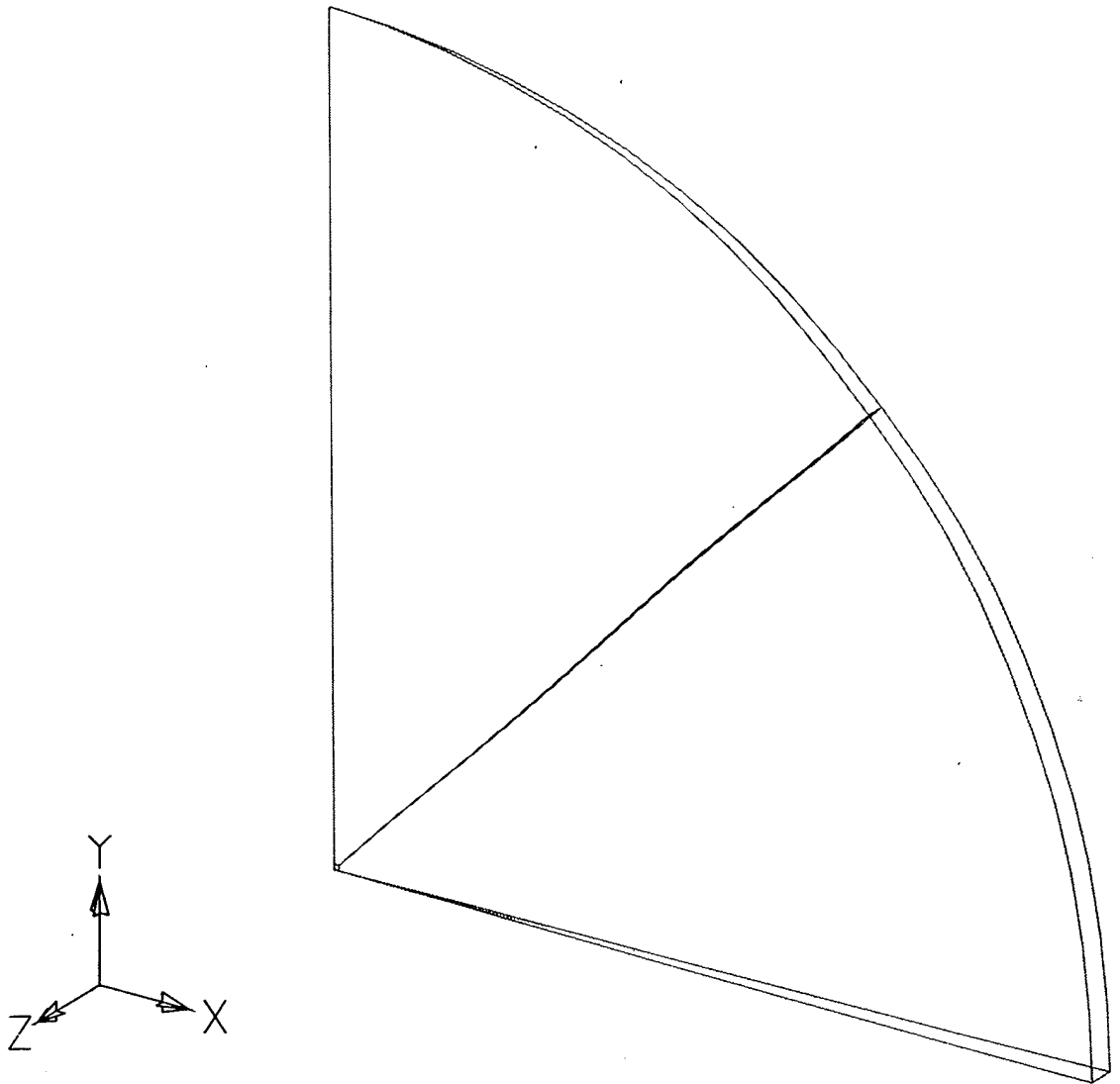
7

Figure 4. Overall Model Geometry for Quarter Symmetry Axisymmetric
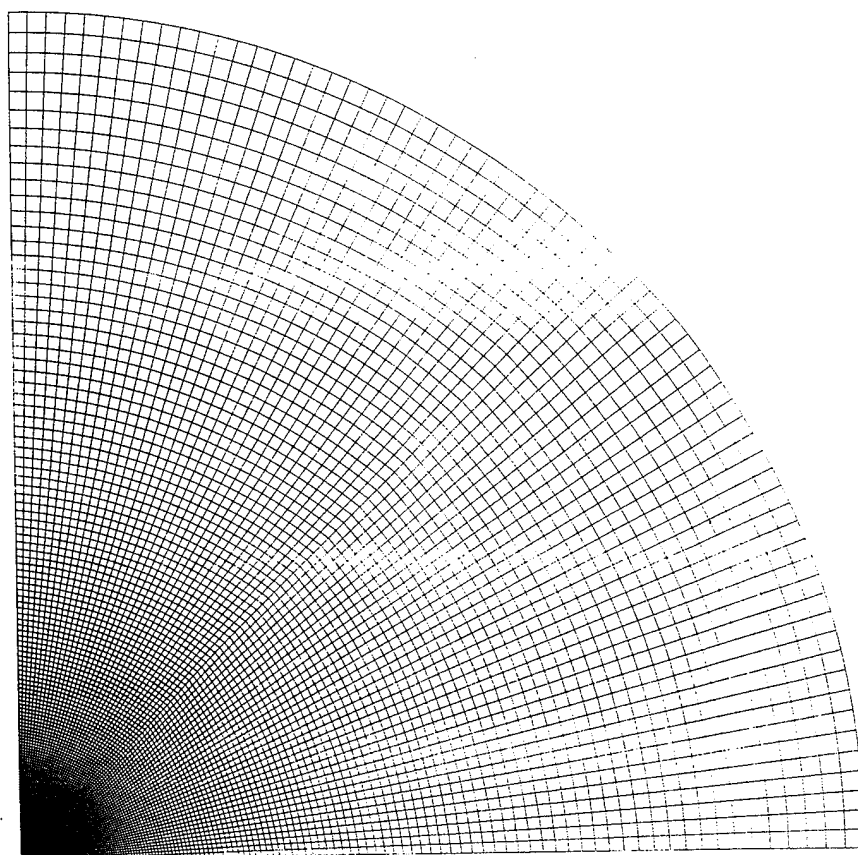
Finite Element Model for Free Field Case

Figure 5. Quarter Symmetry Axisymmetric Finite Element Model for Free Field Case
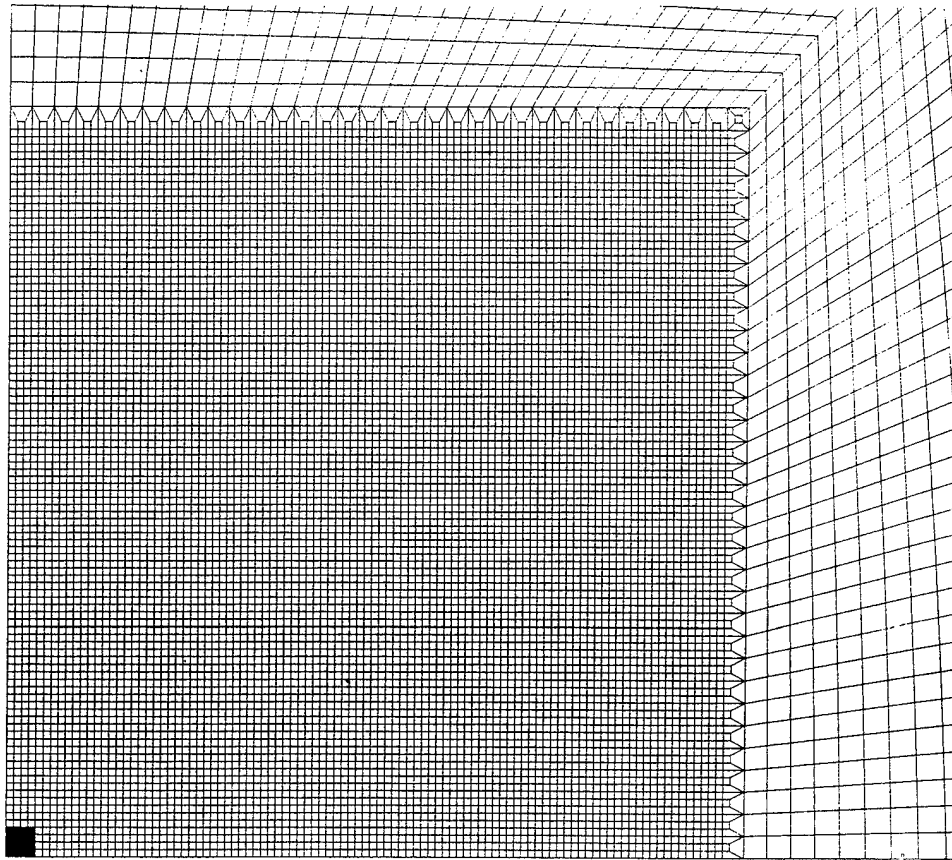
Figure 6.   Close Up View of Finite Element Model in Area near Charge

for Free Field Case

is shown in Figure 6. The black area represent the charge. For simplicity in model generation, the two angled faces in the models which appear to meet at the y-axis are actually offset a very small distance ($\pm 5\mu m$) ;they thus make an angle of ± 1 degree not from the xy-plane at z=0, but from the xy-plane at z=+ $5\mu m$ and z=- $5\mu m$, respectively. This small offset can not be seen on any reasonable scale (it is small even in comparison with the other dimensions of the smallest elements), and permits the model to be meshed using only hexahedron elements.

Figure 7 shows the bubble radius time history. The maximum radius (r_f) is about 0.71m, and the period T_f is about 14.7 milliseconds. Figure 8 shows the total pressure time history. This pressure was measured at 0.71m (same as maximum bubble radius) from the charge center in the horizontal direction. The shock wave pressure and first bubble pulse peak pressure were about 270 MPa and 46 MPa, and occurred at 0.5 and 14.7 milliseconds, respectively. The second and third bubble pulse magnitudes are not clear, but are still higher than the surrounding pressure (10.15 MPa). Empirical equations for TNT [Ref. 1] predict a bubble radius, period and dynamic pressure given by :

maximum bubble radius

$$R_{max} = 3.3825(\frac{W}{D+10})^{\frac{1}{3}} \qquad (m)$$

bubble period

$$T = 2.064\frac{W^{\frac{1}{3}}}{(D+10)^{\frac{5}{6}}} \qquad (second) \qquad\qquad (3)$$

Bubble Radius (cm)
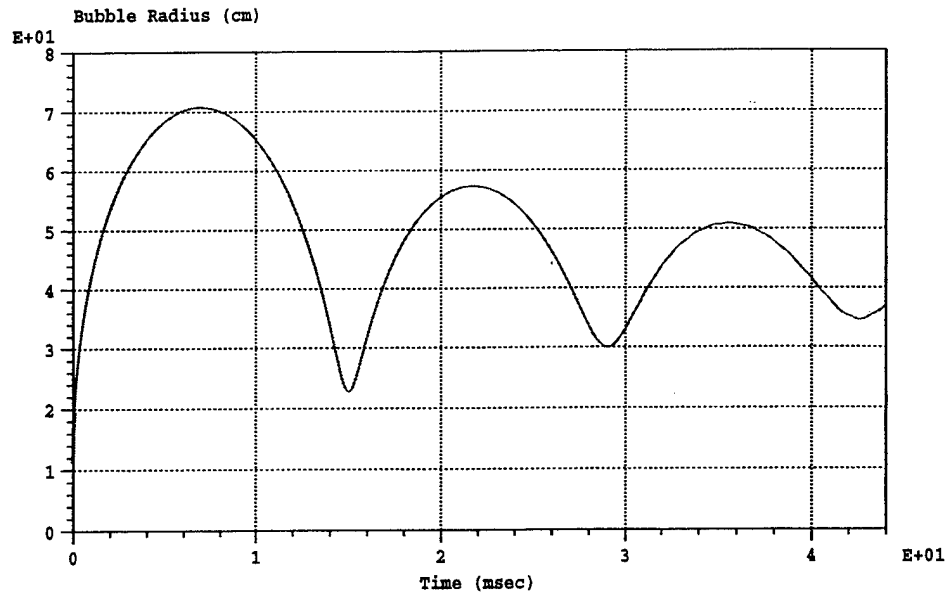
Figure 7.   Bubble Radius Time History for Free Field Case

Total pressure (MPa)
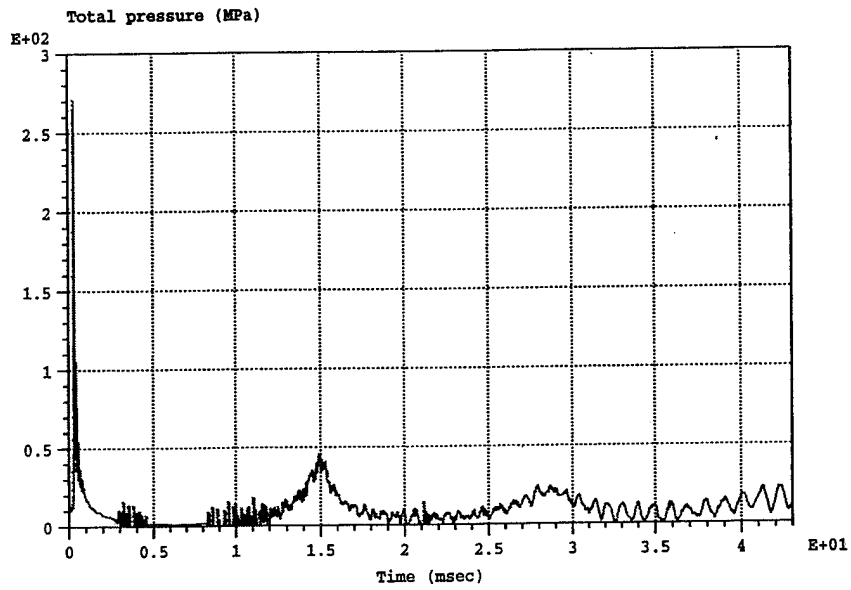
Figure 8.   Pressure Time History for Free Field Case

dynamic pressure

$$P_{max} = 52.118(\frac{W^{\frac{1}{3}}}{L})^{1.18} \qquad \text{(MPa)}$$

<div style="text-align:center">

where   D = charge depth (m)

L = standoff distance (m)

W = charge weight (kg)

</div>

These empirical equations give a maximum bubble radius of 0.71 m, a first oscillation

bubble period of 14.06 milliseconds, and a total shock wave pressure of 205 MPa. These

values are approximate and not much different from the values predicted by the finite

element analysis. Figure 9 shows radial velocities of a fluid particle at the same point

where the pressure was calculated. This computation was done using a spherical wave

equation and the pressure time history given in Figure 8, but using dynamic pressure vice a

total pressure. The spherical wave equation used is shown below [Ref. 5].

$$u_r(t) = u_r(t_0) + \frac{1}{\rho_0 c_0} [p(r,t) - p(r,t_0)] + \frac{1}{\rho_0 r} \int_{t_0}^{t} p(r,T)dT \qquad \text{(4)}$$

where $u_r(t)$ = radial velocity of fluid particle

$u_0(t)$ = initial radial velocity of fluid particle

ρ_0 = initial fluid density (1025 kg/m^3)

c_0 = acoustic velocity in seawater (1500 m/s)

r = standoff distance

p = dynamic pressure

From this equation it is evident that the radial velocity of a fluid particle depends on

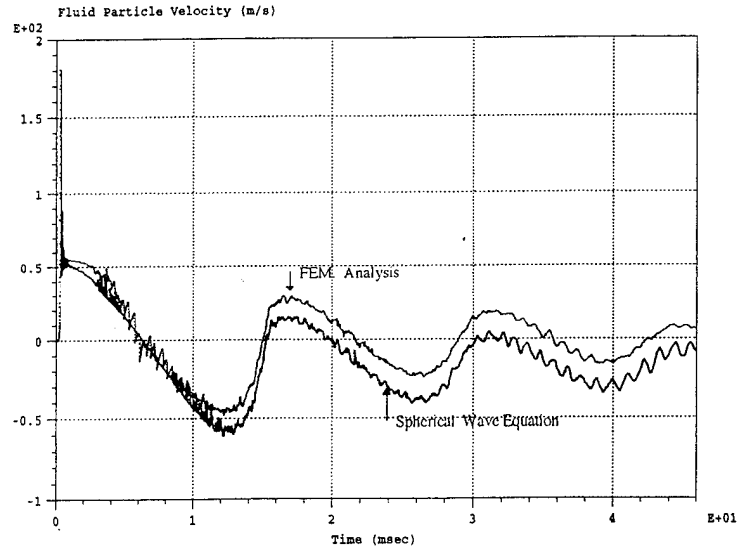both the pressure at that time and the pressure time history.

Figure 9.   Radial Velocity Time History of Fluid Particle for Free Field Case

B.   FLAT RIGID BOUNDARY CASE

Figure 10 shows the bubble problem geometry for the flat rigid boundary case.
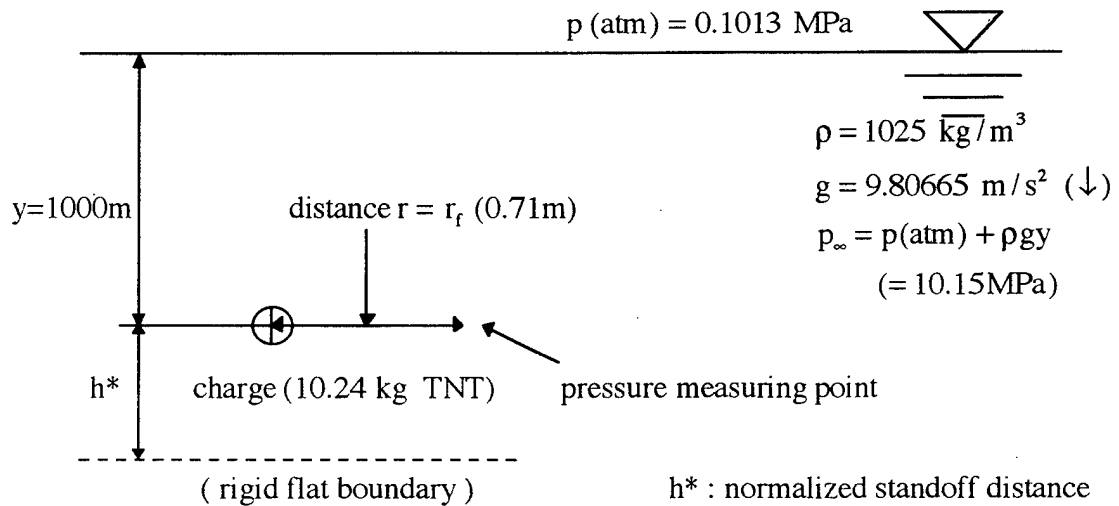

Figure 10.   Bubble Problem Geometry for Flat Rigid Boundary Case

14

The typical overall geometry of a typical finite element model for a flat rigid boundary case, and the complete finite element model, are almost same as shown in the figures for the free field case; the distance from the charge center to the outer boundary is also the same as in the free field case. A view of the finite element model near the charge is shown in Figure 11; the black area represents the charge. The modeling concept is the same as used in the free field case, and was also used for the subsequent cases. In this analysis, the pressure measuring point is same as in the free field case. The distance between the charge center and the rigid boundary surface is defined as a normalized standoff distance $h^* = h / r_f$, where h is the standoff distance from the charge center to the rigid boundary surface, and r_f is the maximum bubble radius for the free field case(0.71 m). Analyses were conducted for h^* values of 1.16 and 2.0 . Obviously, the free field case is the case for which $h^* =$ infinity.

Figure 12 shows the bubble radius time histories for these cases. The maximum bubble radii are 0.67 m for both cases. The first bubble periods (T) for the cases where $h^* = 1.16$ and $h^* = 2$ are 16.6 and 15.5 milliseconds, respectively. The pressure time histories for both cases are shown in Figure 13. The shock wave pressures appear at the same time as in free field case and the magnitudes are also the same. At 1 and 1.7 milliseconds, pressures of 86 and 38 MPa appear in Figure 13 for the cases where $h^* = 1.16$ and 2.0, respectively. Using the empirical equation for pressure and Snell's law to calculate the pressure at the pressure measuring point via bottom reflection, with a constant acoustic velocity in seawater of 1500 m/s, the reflected total pressures are computed as 75.4 and 46.6 MPa for the both cases, and occur at 1.2 and 1.96 milliseconds, respectively. The secondary pressure peaks at 1 and 1.7 milliseconds are therefore bottom reflected
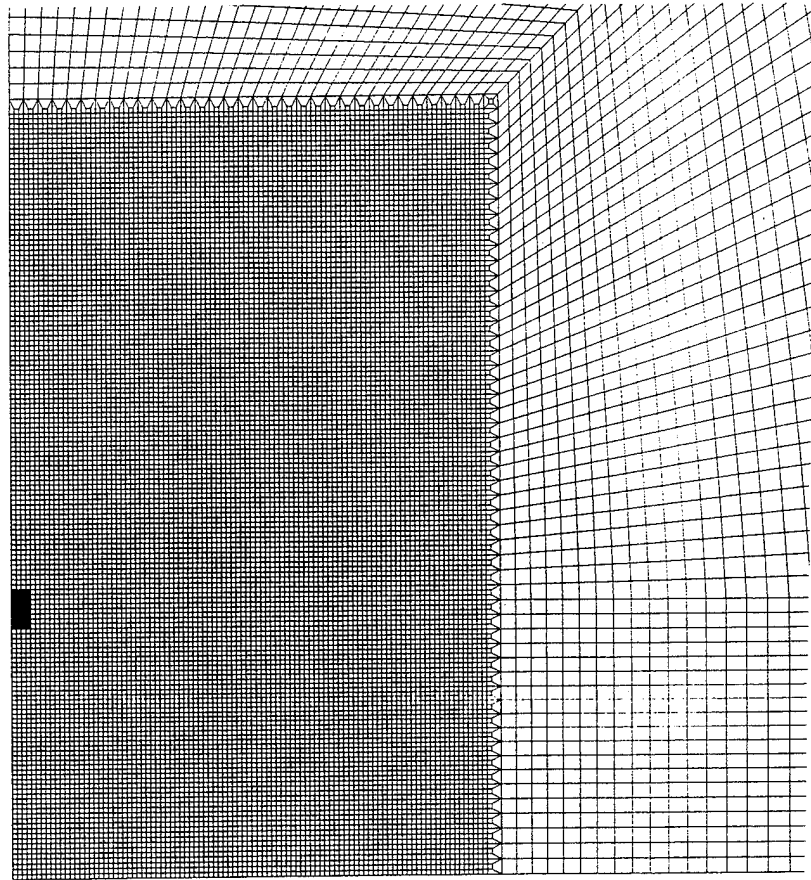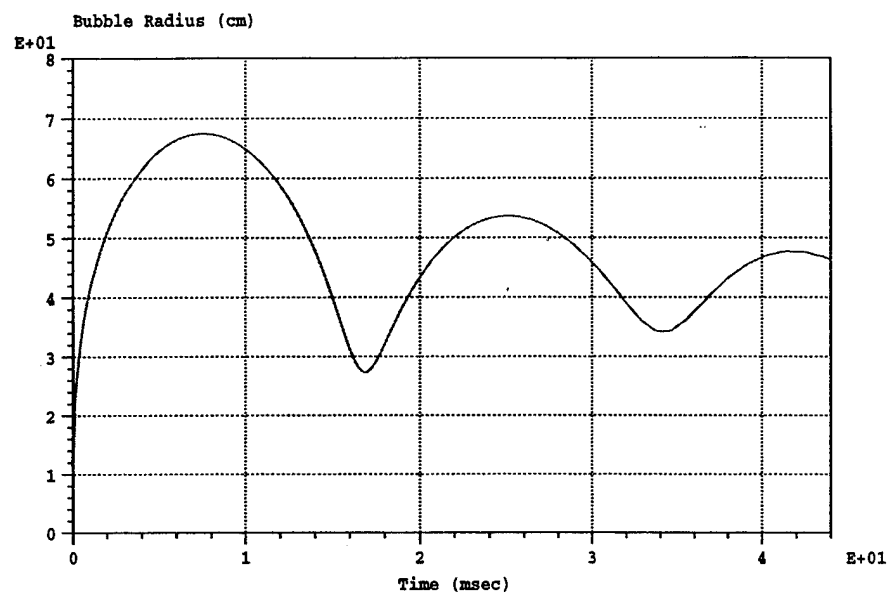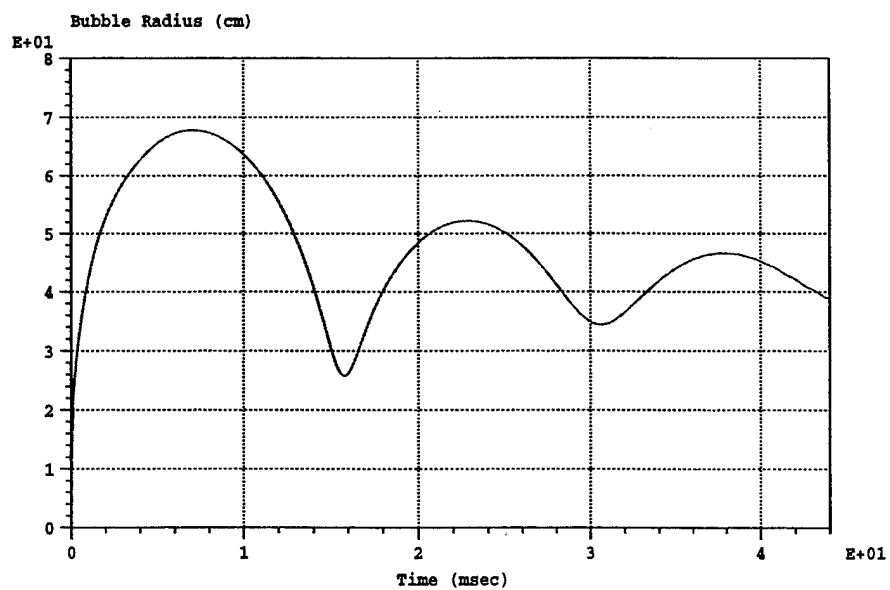
15

Figure 11. Close Up View of Finite Element Model in Area near Charge
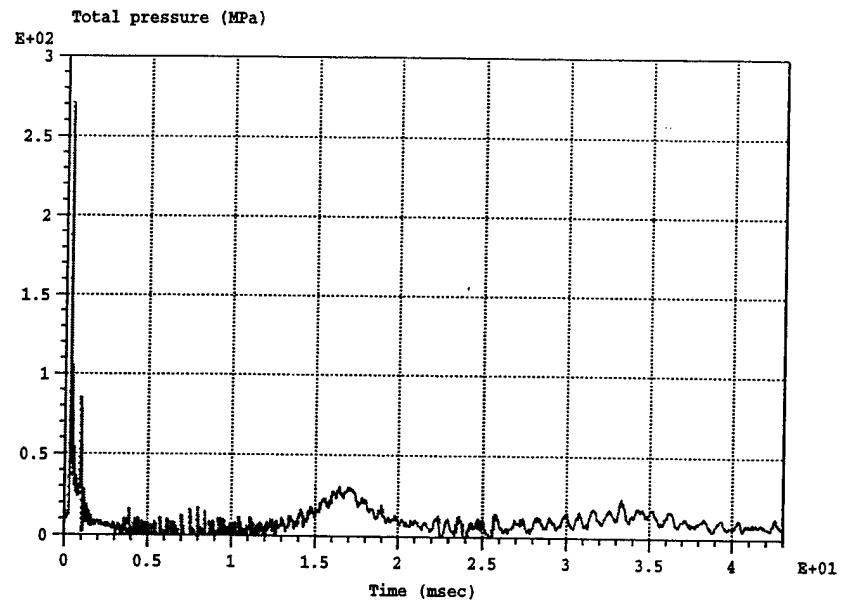
for Flat Rigid Boundary Case

(a)   case for h* = 1.16
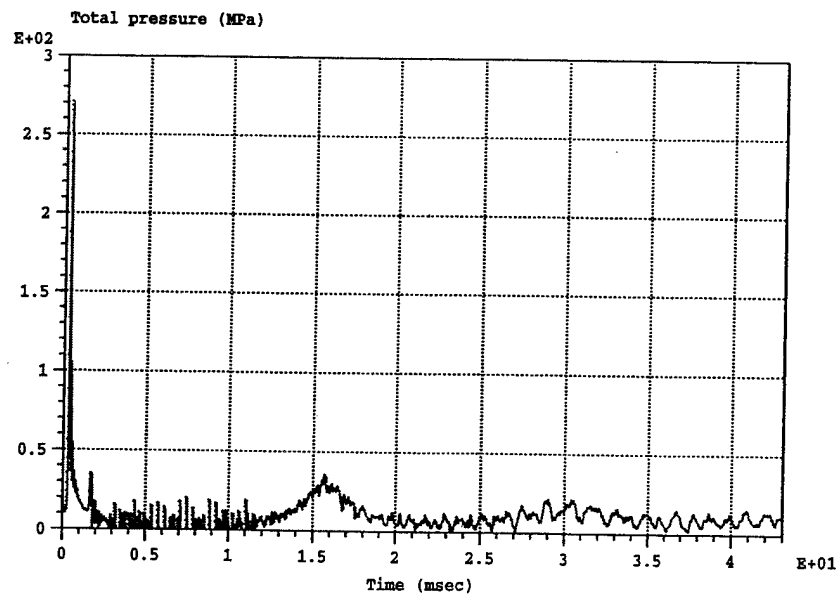

(b)   case for h* = 2.00

Figure 12.   Bubble Radius Time History for Flat Rigid Boundary Case

17

(a)   case for h* = 1.16

(b)   case for h* = 2.00

Figure 13.   Pressure Time History for Flat Rigid Boundary Case

18

pressures. Bubble pulses are 31 and 38 MPa at 16.6 and 15.5 milliseconds. As h^* increases, the maximum bubble radius increases and the bubble period and reflected pressure decrease, approaching the results from the free field case. If standoff distance $h \geq c_0 T_f / 2$, where c_0 is the acoustics wave velocity (1500 m/s) and T_f (14.7 milliseconds) is the bubble period for the free field case, the flat rigid boundary cases will be treated as the free field case. So in cases where $h^* \geq 15.5$ are considered as the free field case. This is because the bubble behavior will not be affected in the first bubble period by the boundary when $h^* \geq 15.5$.

Figure 14 and 15 show the maximum bubble radius, non-dimentionalized dividing by r_f (radius for free field case), and the first bubble period, non-dimentionalized dividing by T_f (period for free field case), versus the normalized standoff distance h^*. The cases for $h^*=1$ and 4 were calculated by Chisum [Ref.2]. In these figures, $h^* = 30$ indicates $h^* =$ infinity.
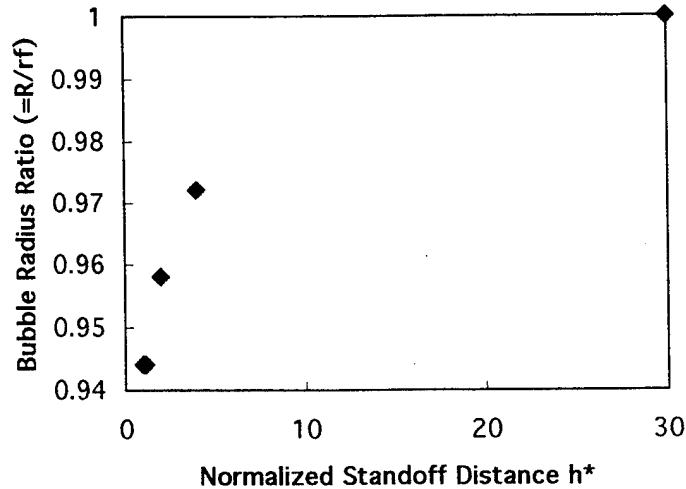

Figure 14. Bubble Radius Ratio vs. Normalized Standoff Distance h^*
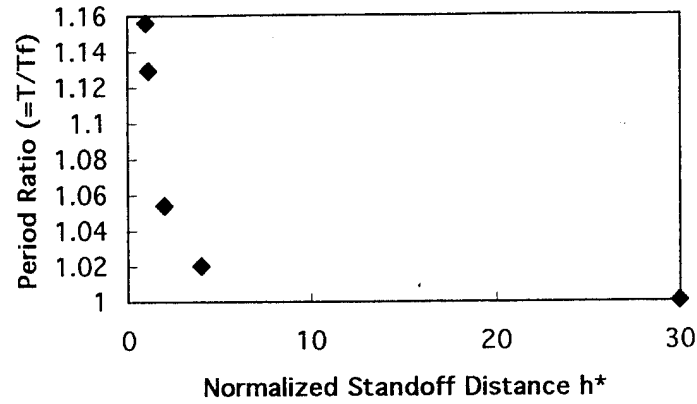for Flat Rigid Boundary Case

19

Figure 15. Period Ratio vs. Normalized Standoff Distance h*
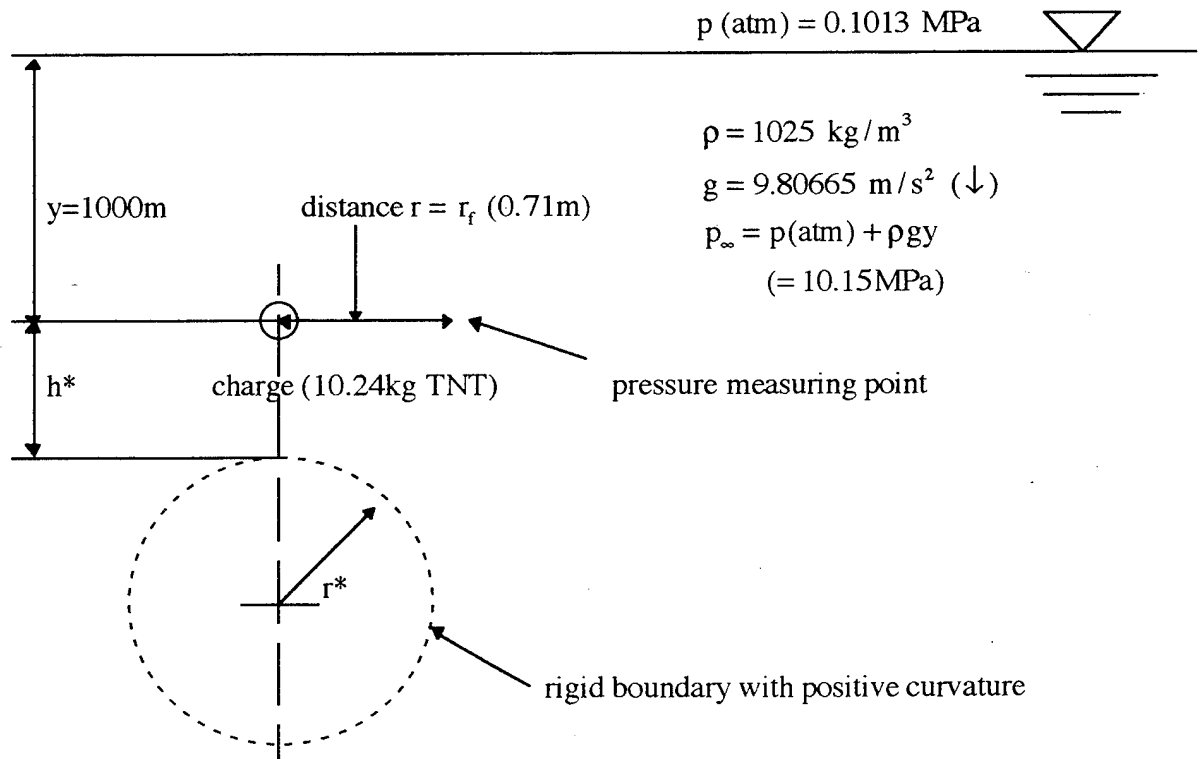for Flat Rigid Boundary Case

Figure 16. Bubble Problem Geometry for Rigid Boundary Case

with Positive Curvature

20

C. CURVED RIGID BOUNDARY CASE

1. Cases With Positive Curvature

Figure 16 shows the bubble problem geometry for a rigid boundary case with positive curvature. The finite element model for an axisymmetric rigid boundary with positive curvature case is shown Figure 17. The distance from the charge center to the outer boundary is 400m. Figure 18 shows the "central" region of the model; black area represents the charge. The empty semi-circular arc represents the boundary surface with a normalized arc radius of $r* = R / r_f$ where R is the actual arc radius. Analyses were conducted for in which $r*$ is equal to 1, 2, 4 and 10, and the normalized standoff distance $h*$ is 2.

The bubble radius time histories for each case were shown in Figure 19. Table 1 lists the maximum bubble radius and bubble period. Figure 20 shows the pressure time histories. Table 2 indicates the shock wave pressure, reflected pressure and first bubble pulse. In these analyses, the bubble acts like the free field case when $r*$ is less than 2. As $r*$ increases, the bubble behaves like the flat rigid boundary case with the same $h*$.

Figure 21 and 22 are rearranged to show the maximum bubble radius and first period, non-dimentionalized by dividing by r_f (radius for free field case) and dividing by T_f (period for free field case), respectively, versus the normalized arc radius $r*$. In these figures, $r* = 30$ indicates $r* = $ infinity.
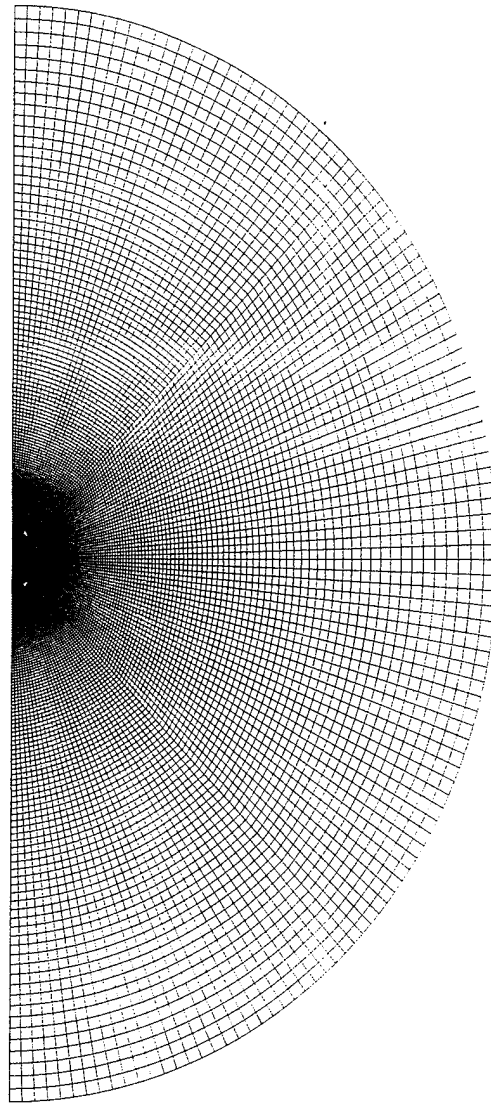
Figure 17.   Axisymmetric Finite Element Model for Rigid Boundary Case
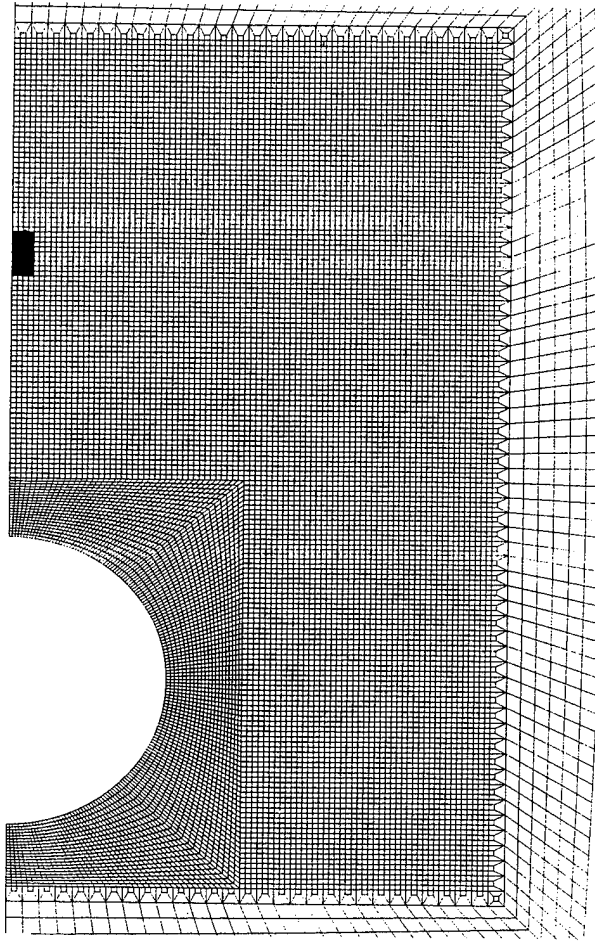with Positive Curvature

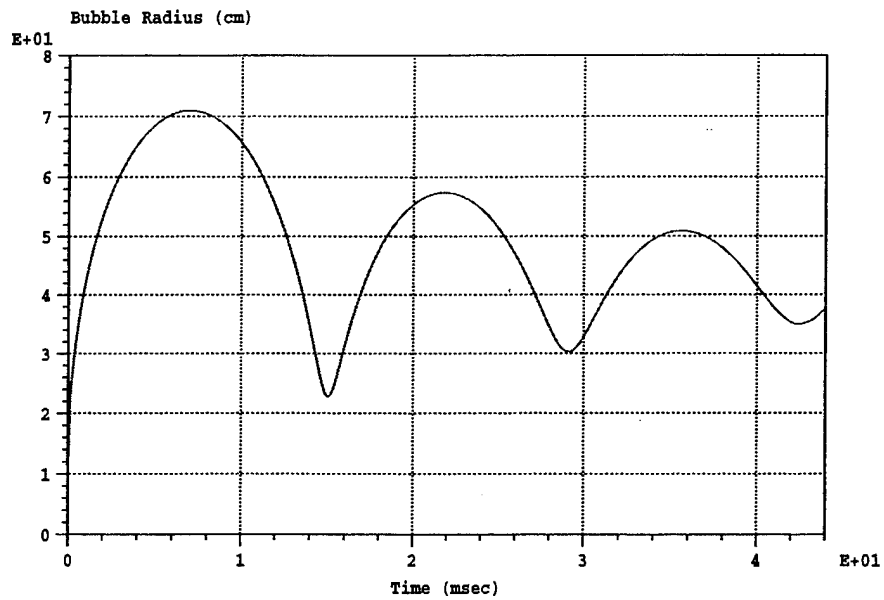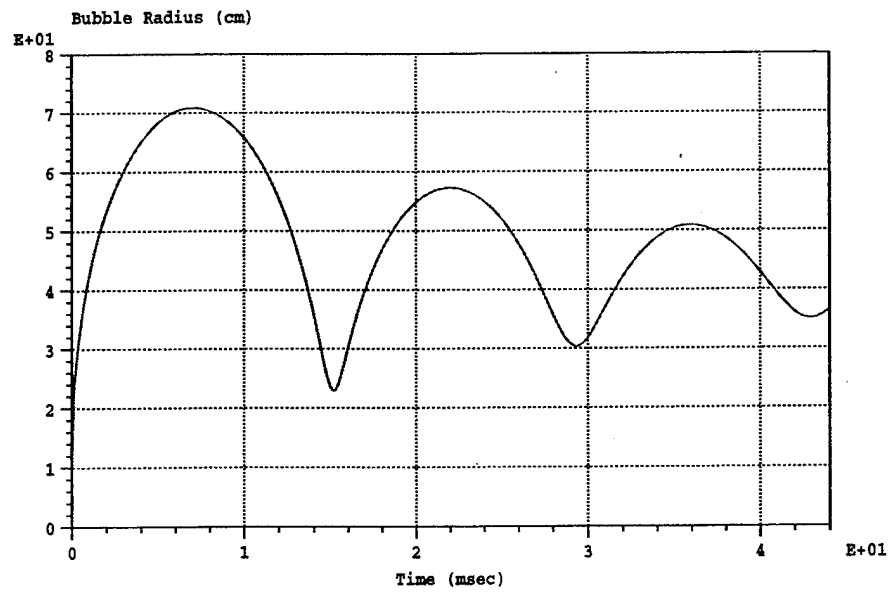Figure 18.   Close Up View of Finite Element Model in Area near Charge
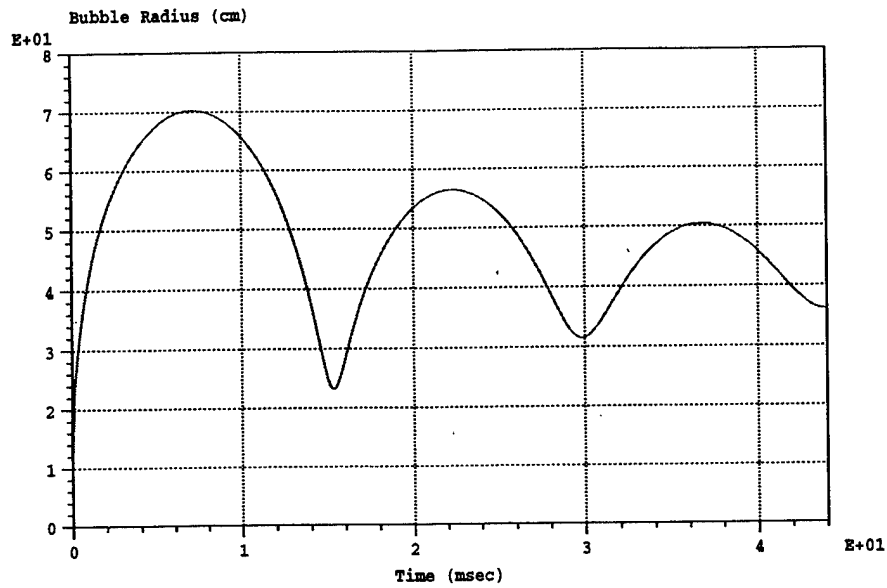
for Rigid Boundary Case with Positive Curvature

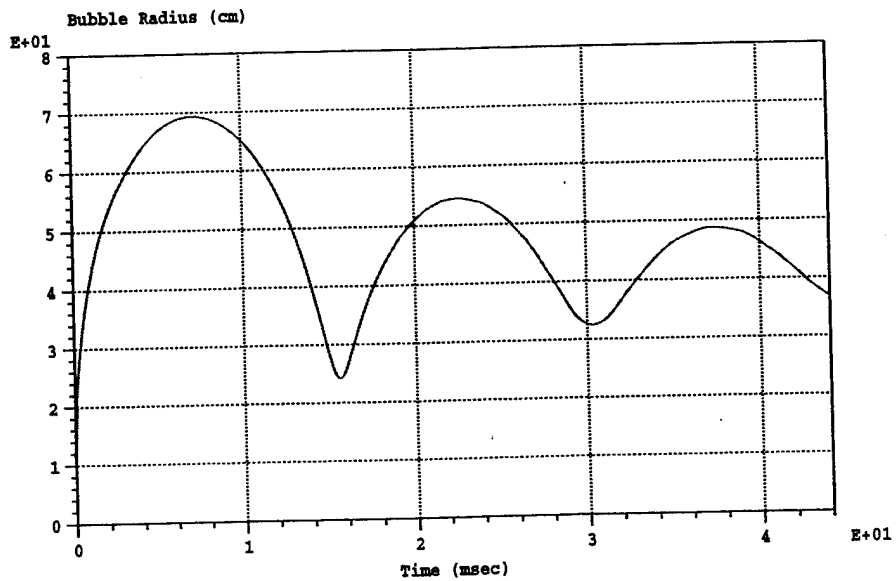Bubble Radius (cm)

(a)   case for r* = 1, h* = 2

Bubble Radius (cm)

(b)   case for r* = 2, h* = 2

Figure 19-1.   Bubble Radius Time History for Rigid Boundary Case
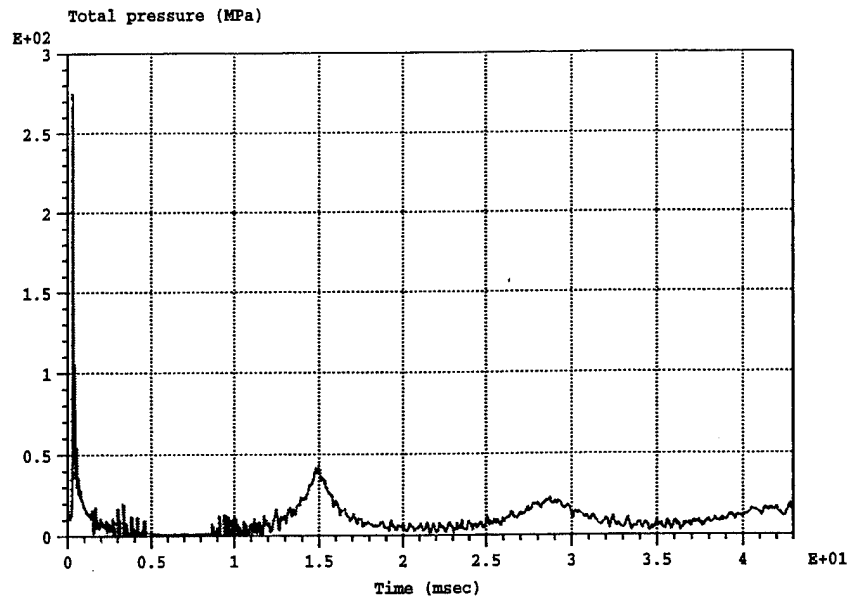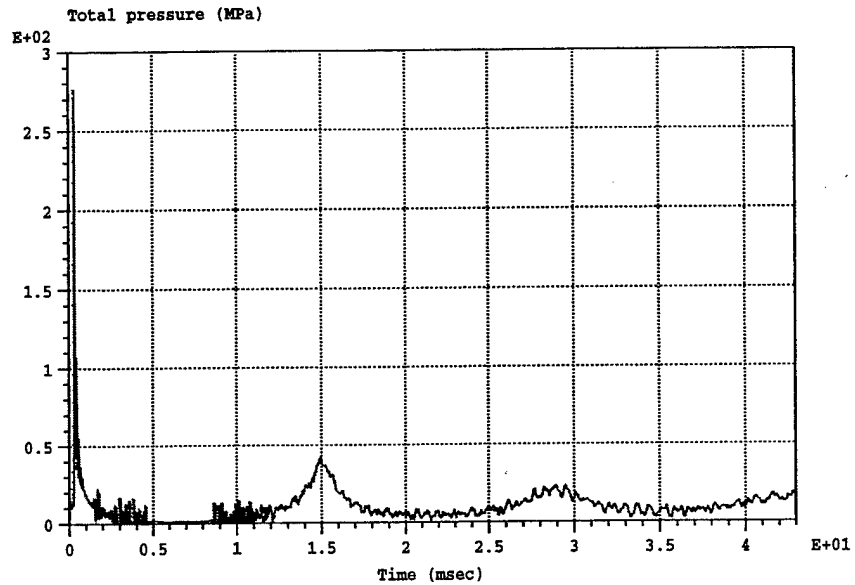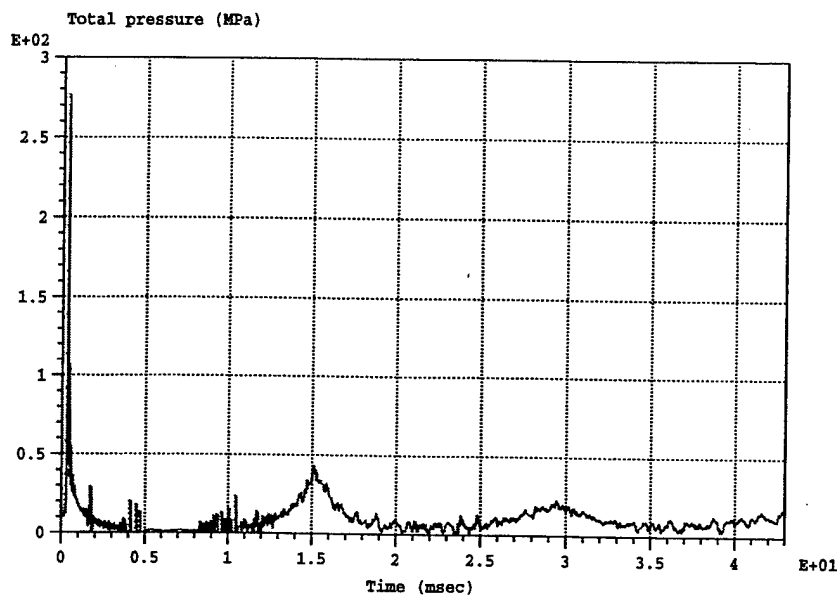with Positive Curvature

Bubble Radius (cm)

(c)   case for r* = 4, h* = 2

Bubble Radius (cm)

(d)   case for r* = 10, h* = 2

Figure 19-2.   Bubble Radius Time History for Rigid Boundary Case
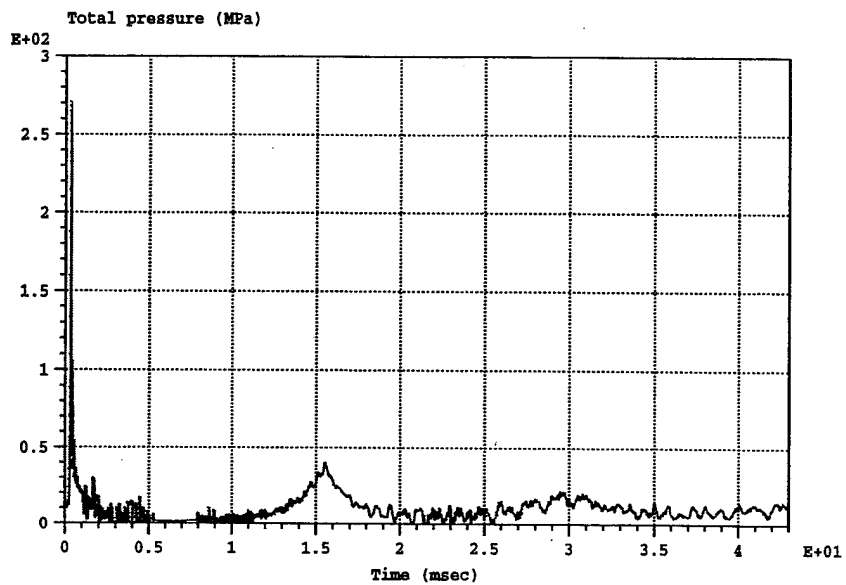with Positive Curvature

Total pressure (MPa)

(a)   case for r* = 1, h* = 2

Total pressure (MPa)

(b)   case for r* = 2, h* = 2

Figure 20-1.   Pressure Time History for Rigid Boundary Case
with Positive Curvature

26

Total pressure (MPa)

(c)   case for r* = 4, h* = 2

Total pressure (MPa)

(d)   case for r* = 10, h* = 2

Figure 20-2.   Pressure Time History for Rigid Boundary Case
               with Positive Curvature

Table 1. Max. Bubble Radius and First Bubble Period for Positive Curvature

r*	max. bubble radius (m)	first bubble period (msec)	note
0	0.71	14.7	free field case
1	0.71	14.7	h*=2
2	0.71	14.8	h*=2
4	0.70	15.0	h*=2
10	0.68	15.3	h*=2
infinity	0.67	15.5	flat boundary (h*=2)

Table 2. Shock Wave, Reflected Pressure and Bubble Pulse for Positive Curvature

r*	shock wave pressure (MPa)	reflected pressure (MPa)	bubble pulse (MPa)	note
0	270	none	46	free field case
1	275	unknown	45	h* = 2
2	277	23	44	h* = 2
4	277	30	44	h* = 2
10	270	30	40	h* = 2
infinity	270	38	38	flat boundary (h* = 2)
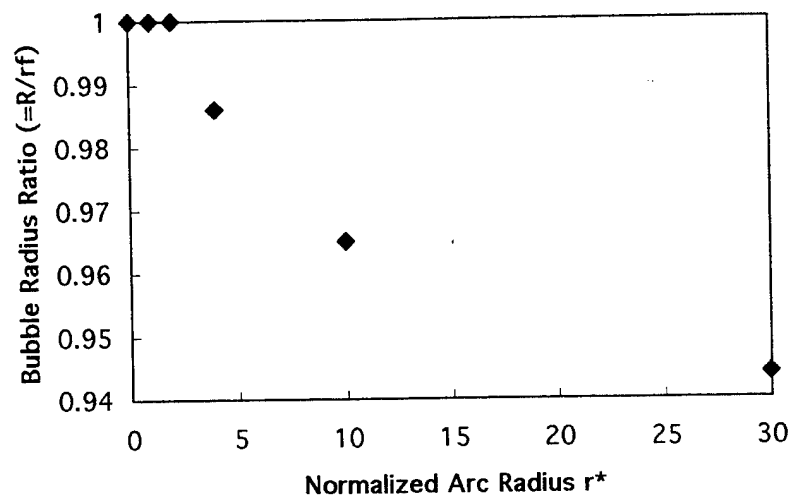
Figure 21. Bubble Radius Ratio vs. Normalized Arc Radius r* for Case
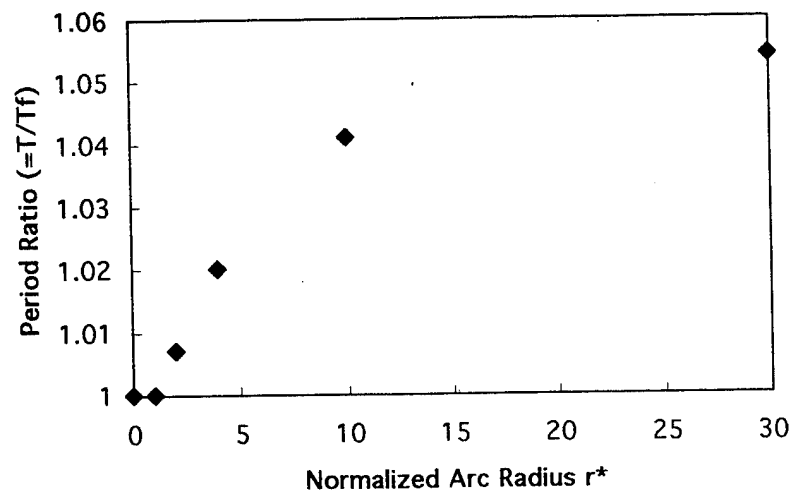
with Positive Curvature

Figure 22.   Period Ratio vs. Normalized Arc Radius r* for Case with Positive Curvature

2. Cases With Negative Curvature

Figure 23 shows the bubble problem geometry for a rigid boundary case with negative curvature. The finite element model for an axisymmetric rigid boudary with negative curvature is shown Figure 24. In this case, the charge is enclosed by the curved rigid boundary and the distance from the charge center to the boundary is not 400m. Figure 25 shows the "central" region of the model; black area represents the charge. Analyses were conducted for values of r^* is equal to 4, 7, 9 and 13, and a normalized standoff distance h^* is 2.

The bubble radius time histories for each case are shown in Figure 26. Table 3 lists the maximum bubble radius and first bubble period for each case. Figure 27 shows the pressure time histories. Table 4 indicates the shock wave pressure, reflected pressure and first bubble pulse.

In these analyses, the charge was enclosed by a rigid boundary and distance from the charge to the boundary was very small compared to the other cases in which the distance was 400m. (note that the case when $r^* = 0$ is impossible) For the negative curvature boundary cases , the results are affected by multiple reflection paths. This is already seen in the graph for the $r^* = 4$ case where there is a large amount of "noise". In the $r^* = 4$ case, the boundary is so close that it significantly effects bubble growth and collapse. As r^* increases, the bubble radius and the bubble period are seen to increase, approaching the flat boundary case results for large r^* values, as expected.

30

p (atm) = 0.1013 MPa

$\rho = 1025 \ kg/m^3$

$g = 9.80665 \ m/s^2 \ (\downarrow)$

$p_\infty = p(atm) + \rho gy$

$(= 10.15 MPa)$

$r^* = R/r_f$: R = curvature radius

y=1000m

distance r = r_f (0.71m)   rigid negative curvature

r*
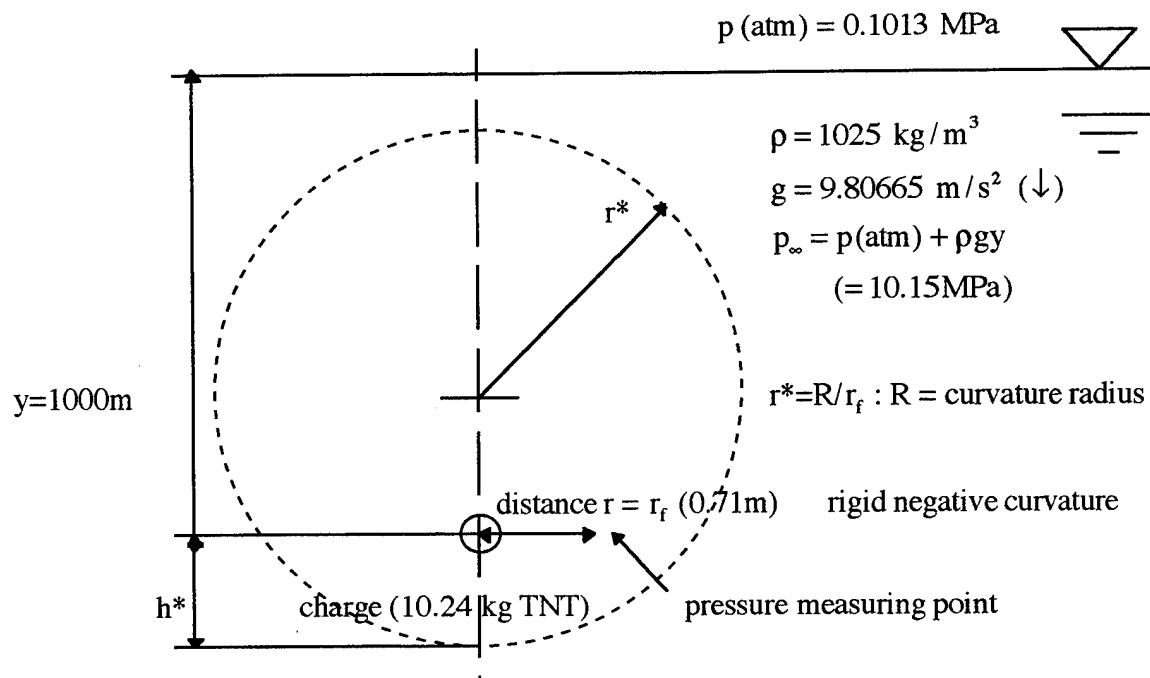
h*   charge (10.24 kg TNT)   pressure measuring point

Figure 23. Bubble Problem Geometry for Rigid Boundary Case
with Negative Curvature

Table 3. Max. Bubble Radius and First Bubble Period for Negative Curvature

r*	max. bubble radius (m)	first bubble period (msec)	note
none	0.71	14.7	free field case (reference)
4	0.54	7.6	h*=2
7	0.62	12.7	h*=2
9	0.64	14.2	h*=2
13	0.66	15.2	h*=2
infinity	0.67	15.5	flat boundary (h*=2)
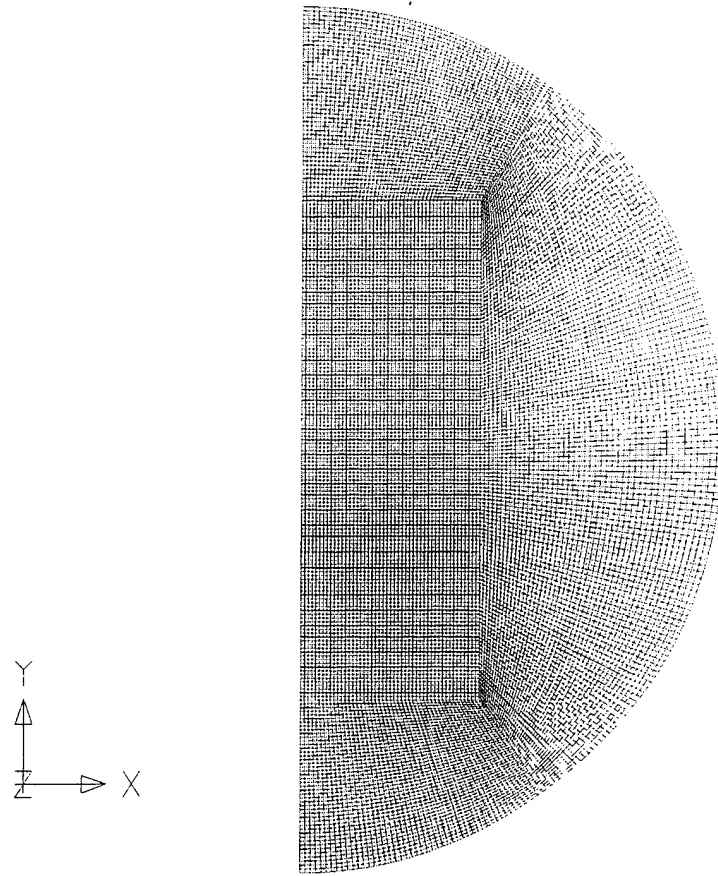
Figure 24. Axisymmetric Finite Element Model for Rigid Boundary Case

with Negative Curvature
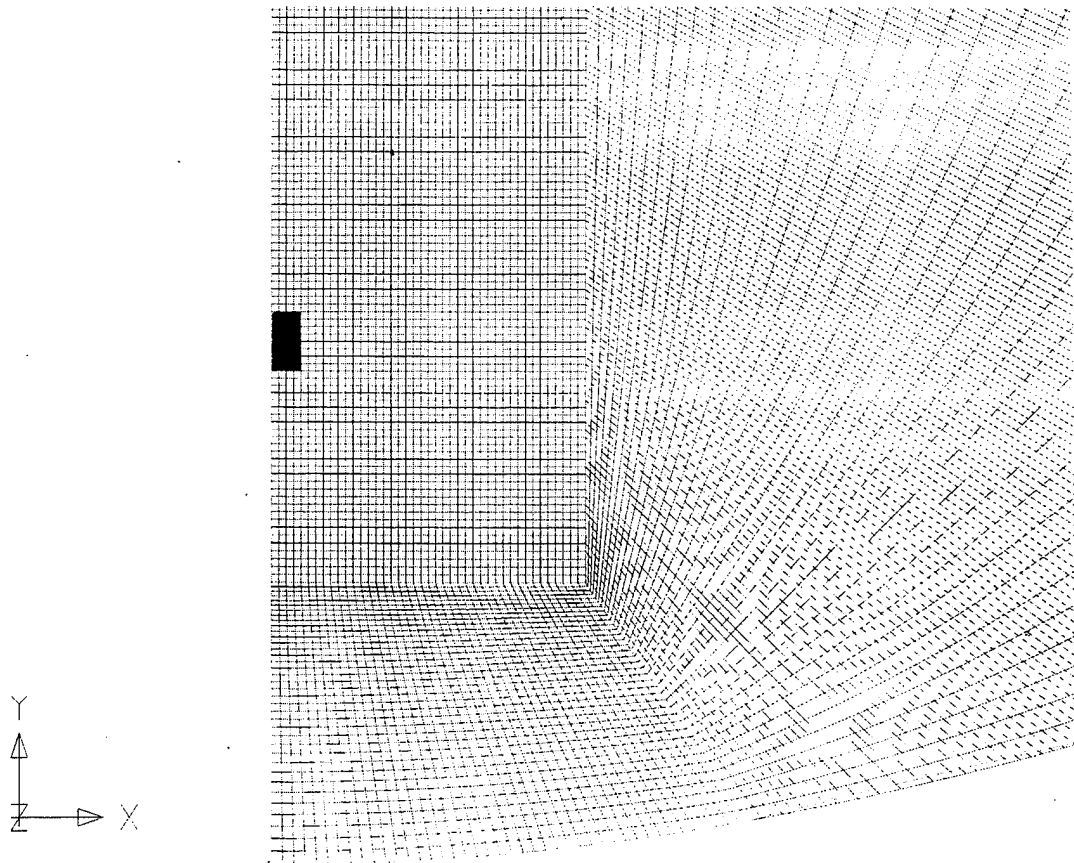
Figure 25.   Close Up View of Finite Element Model in Area near Charge

for Rigid Boundary Case with Negative Curvature

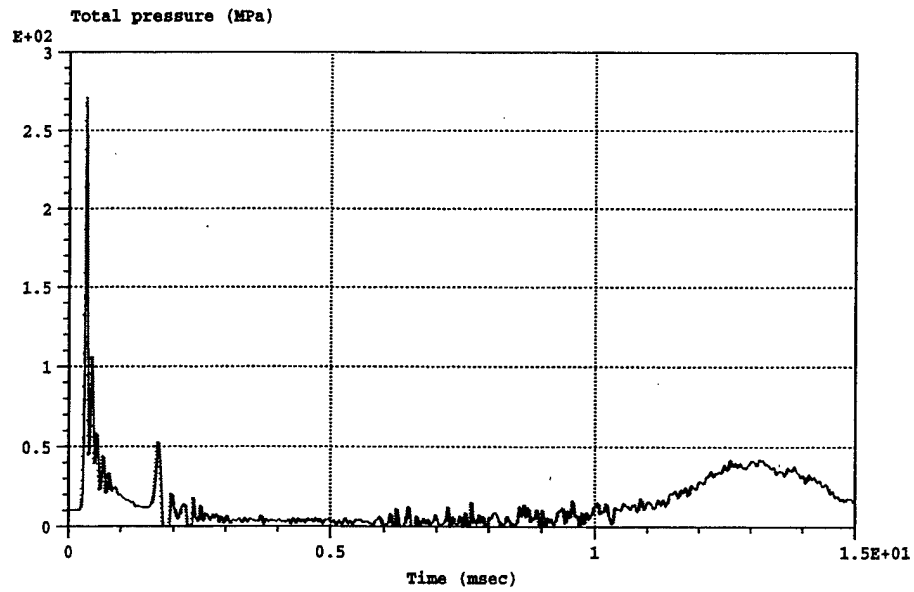**Bubble Radius (cm)**

(a)   case for r* = 4, h* = 2
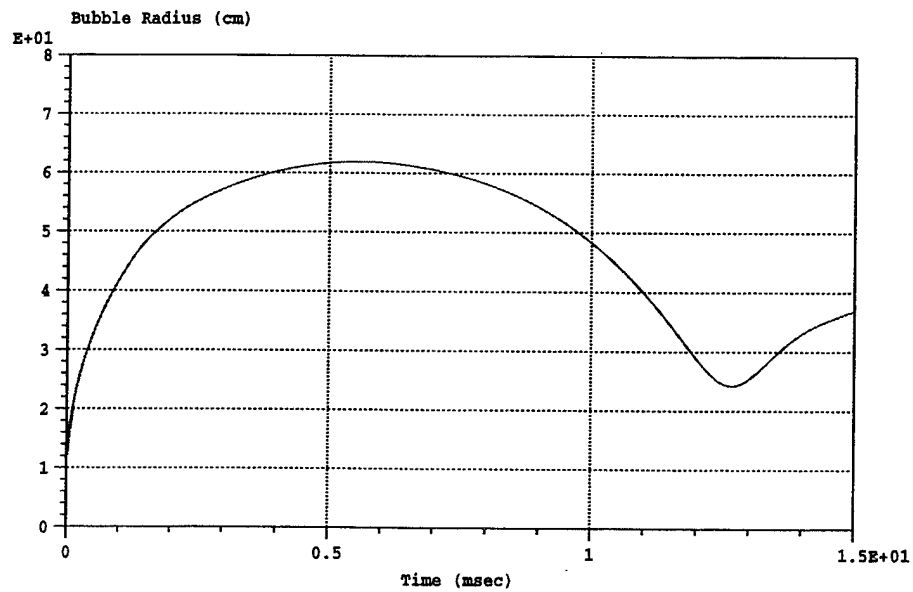
Bubble Radius (cm)

(b)   case for r* = 7, h* = 2

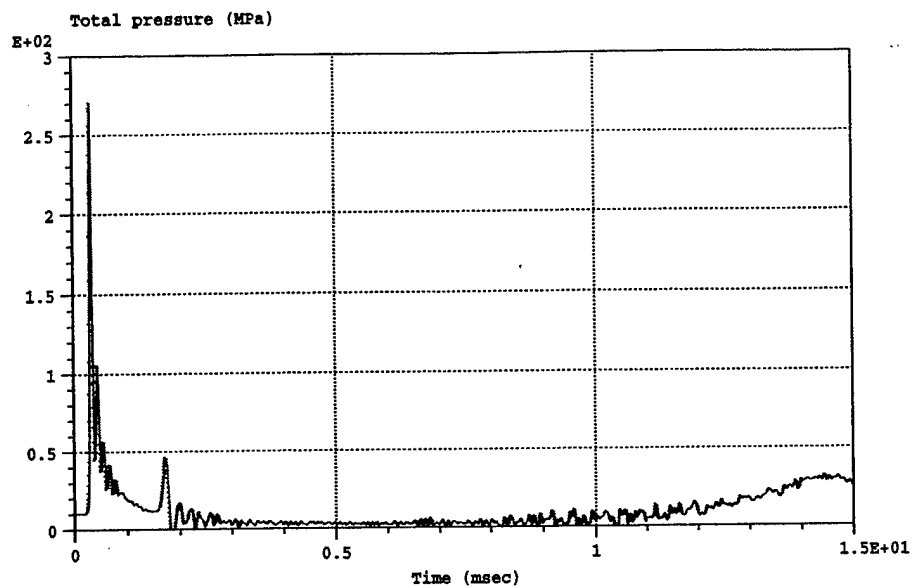Figure 26-1. Bubble Radius Time History for Rigid Boundary Case
with Negative Curvature

34

Bubble Radius (cm)
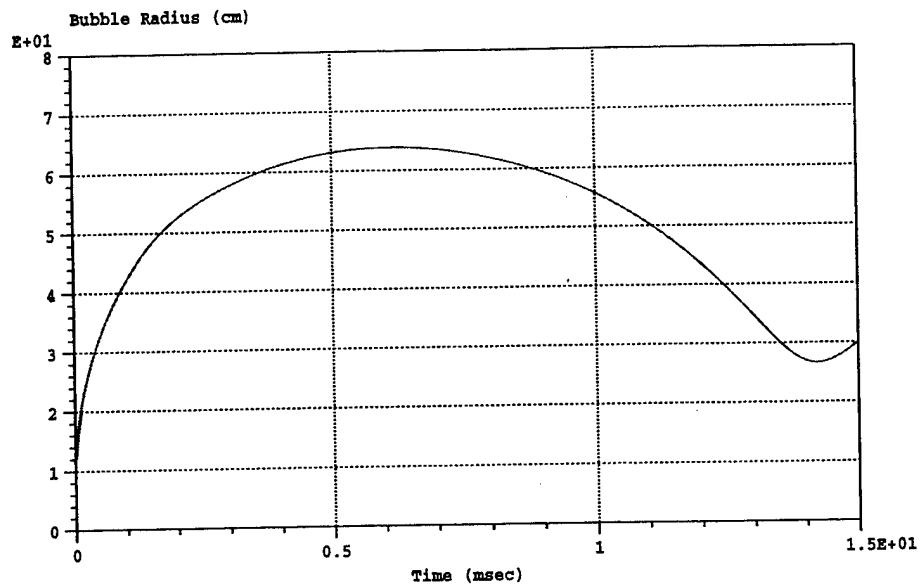
(c)   case for r* = 9, h* = 2
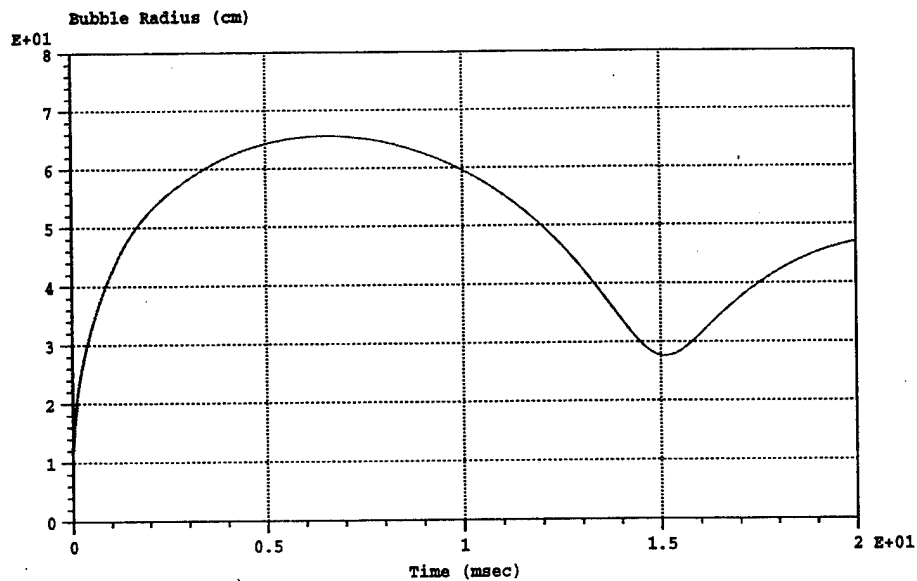
Bubble Radius (cm)

(d)   case for r* = 13, h* = 2

Figure 26-2.   Bubble Radius Time History for Rigid Boundary Case
with Negative Curvature

35
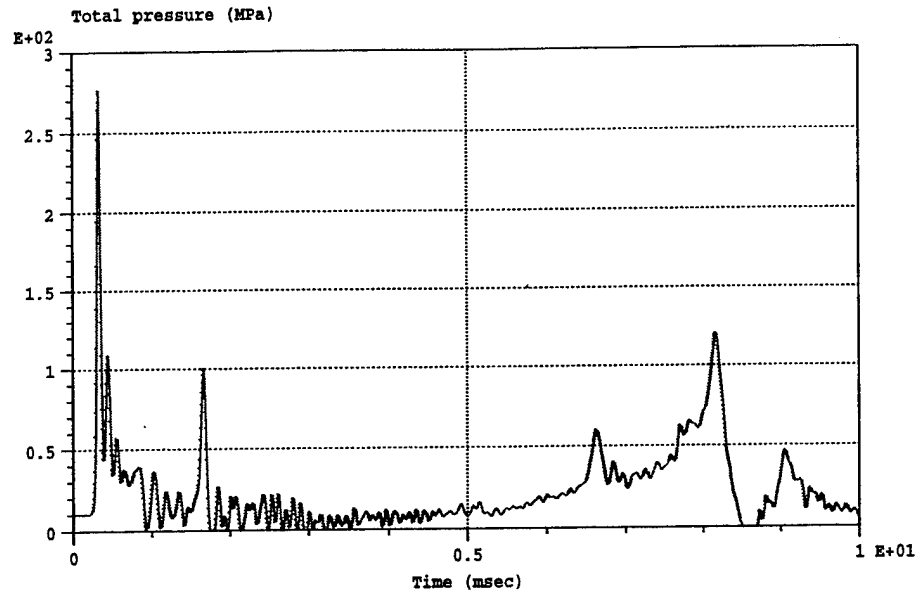
(a)   case for r* = 4, h* = 2

(b)   case for r* = 7, h* = 2

Figure 27-1.   Pressure Time History for Rigid Boundary Case
with Negative Curvature

Total pressure (MPa)

(c) case for r* = 9, h* = 2
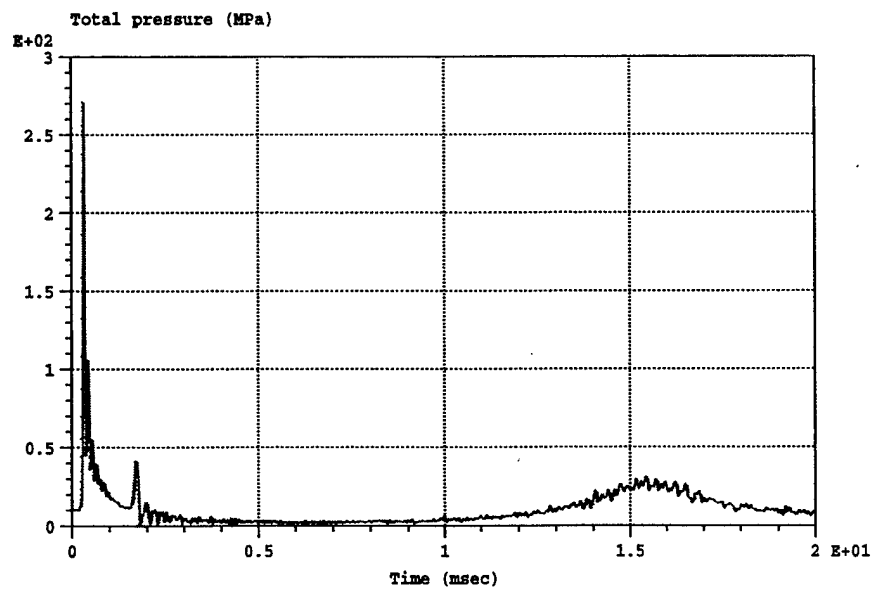
Total pressure (MPa)

(d) case for r* = 13, h* = 2

Figure 27-2. Pressure Time History for Rigid Boundary Case
with Negative Curvature

37

Table 4   Shock Wave, Reflected Pressure and Bubble Pulse for Negative Curvature

r*	shock wave pressure (MPa)	reflected pressure (MPa)	bubble pulse (MPa)	note
none	270	none	46	free field case (reference)
4	278	100	123	h* = 2
7	270	52	41	h* = 2
9	270	47	33	h* = 2
13	270	40	40	h* = 2
infinity	270	38	38	flat boundary (h* = 2)

Figures 28 and 29 show the non-dimentionalized bubble radius and period as a function of the normalized arc radius r*. In these figures, h* = 30 indicates h* = infinity.

D.   BUBBLE SHAPE

The shapes of the bubble for the free field case, the flat rigid boundary cases with h* = 1.16 and 2 and the case with positive boundary curvature with r* = 10 and h* = 2 are plotted in Appendix A at times t of 0.0, 0.50, 0.80, 0.90 0.95, 0.98, 0.99, and 1.00T, where T is the first bubble period for each case. The free field case and the rigid boundary cases with h* = 2 have similar shapes in which the bubble remains nearly spherical up to 1.00T. The case with h* = 1.16 shows a heart shaped bubble after time 0.90T. The center

38

of mass of the bubble in this case is also seen to move closer to the boundary at late times. These related phenomena are due to the effect of the boundary on the fluid flow surrounding the charge.
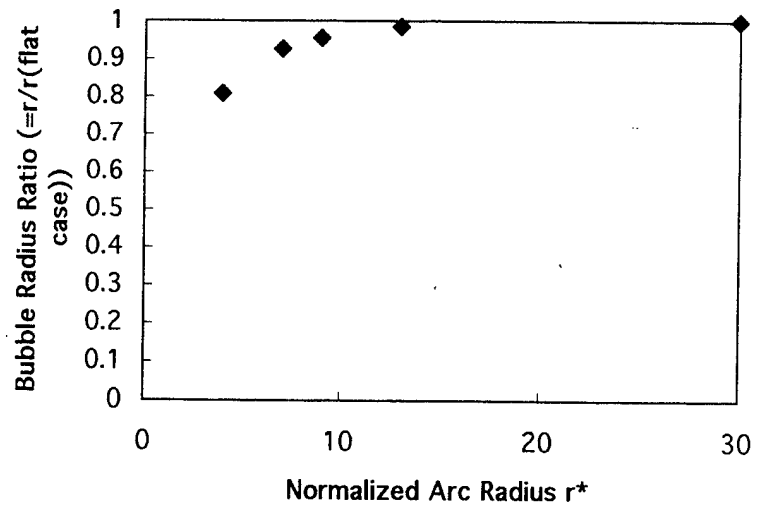
Figure 28. Bubble Radius Ratio vs. Normalized Arc Radius r*

for Case with Negative Curvature
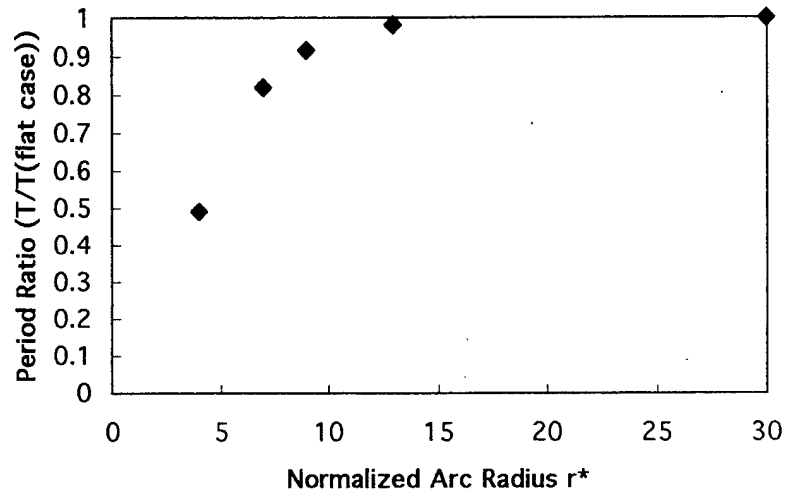
Figure 29. Period Ratio vs. Normalized Arc Radius r* for Case with Negative Curvature

IV. CONCLUSION

A.   FREE FIELD CASE

The free field case gives the basic information about the bubble behavior in an underwater explosion. The empirical equations are valid for this case, and the spherical wave equation can be used to calculated the fluid particle velocity with reasonable accuracy.

B.   FLAT RIGID BOUNDARY CASE

The flat rigid boundary case is a special case of a curved rigid boundary case with the normalized arc radius r * equal to infinity. The normalized standoff distance h* affects the bubble behavior significantly. As h* increases, the bubble behavior approaches that of the free field case.   If the standoff distance $h \geq c_0 T_f / 2$, there is no boundary effect. When h* is small enough, the bubble is attracted to the boundary surface and the bubble becomes heart shaped during late stages of the bubble collapse.

C.   CURVED RIGID BOUNDARY CASE

1.   Positive Curvature

In this case, the normalized arc radius r* influences the bubble behavior. When r* is small enough, the bubble behavior is similar to the free field case. And as r* increases, the bubble behaves as in the flat rigid boundary case.

2. Negative Curvature

The normalized arc radius r* has a similar effect upon the behavior of the bubble as in the positive curvature case. However when r* is small, there are multiple reflection paths which effect the bubble and make the analysis of this case complicated.

V. RECOMMENDATION

This paper describes the effects of rigid boundary curvature on the bubble behavior in an underwater explosion. Since the boundary is rigid, this does not represent an actual case. Next time, the flexible boundary case needs to be investigated.

APPENDIX : BUBBLE SHAPES
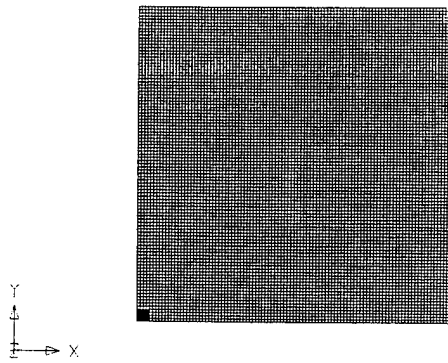
(a) at Time = 0.0T
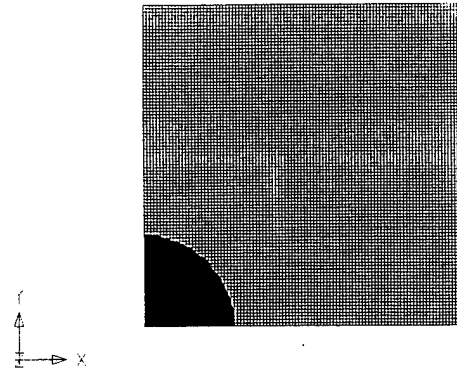
(b) at Time = 0.50T
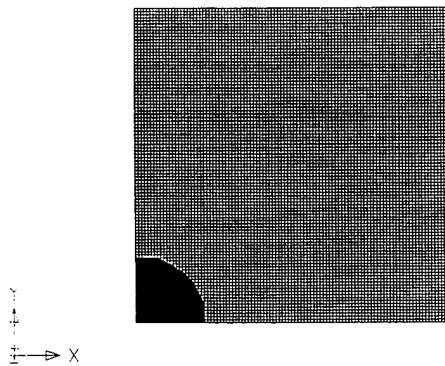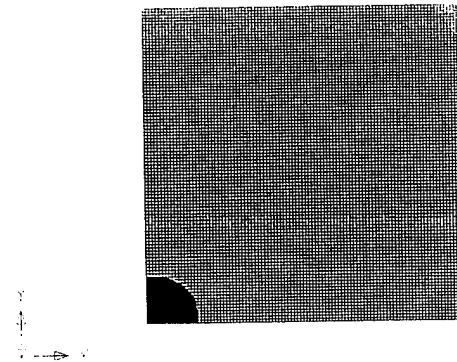
(c) at Time = 0.80T

(d) at Time = 0.90T

Figure 30-1.   Bubble Shape for Free Field Case
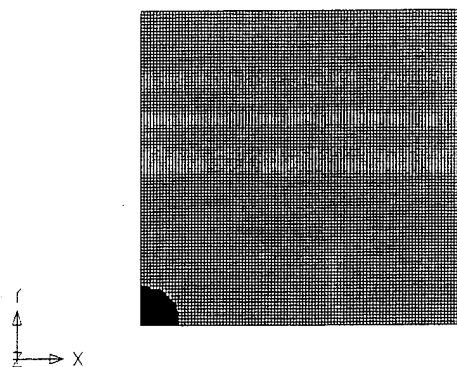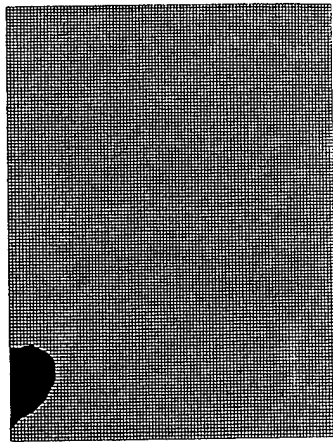
(a) at Time = 0.95T
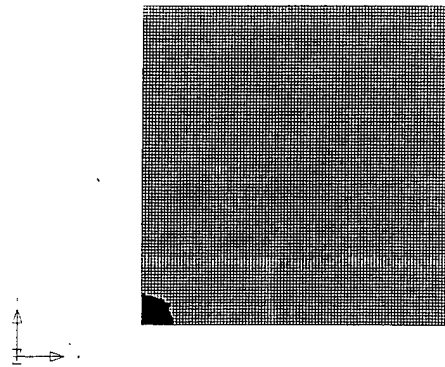
(b) at Time = 0.98T
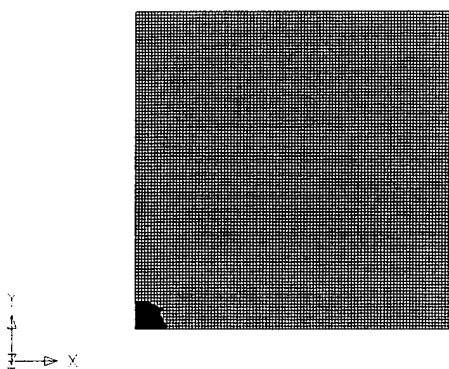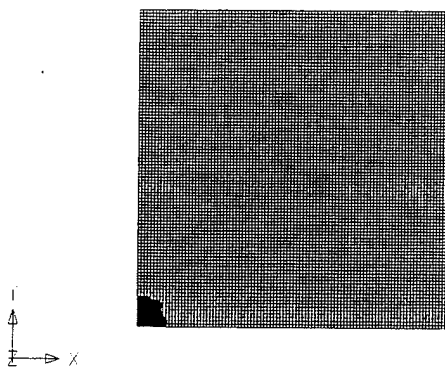
(c) at Time = 0.99T

(d) at Time = 1.00T

Figure 30-2.   Bubble Shape for Free Field Case
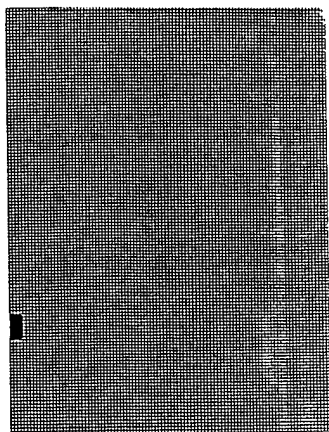
(a) at Time = 0.0T
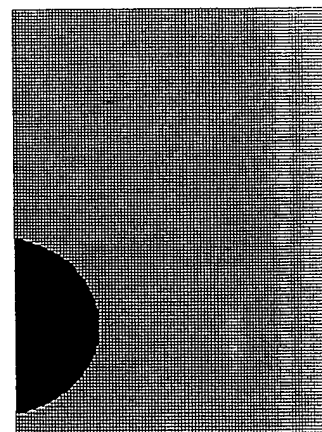
(b) at Time = 0.50T
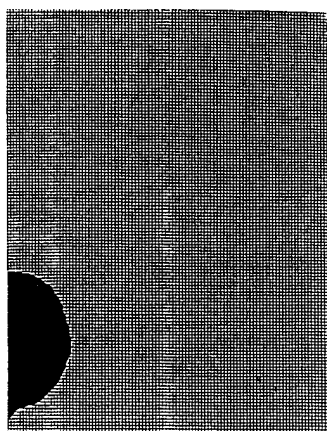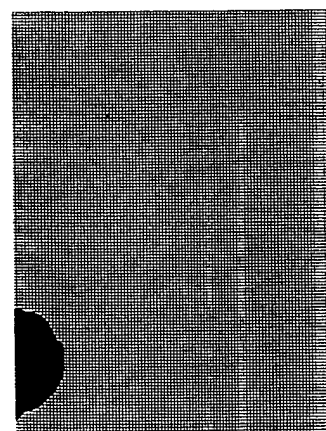
(c) at Time = 0.80T

(d) at Time = 0.90T

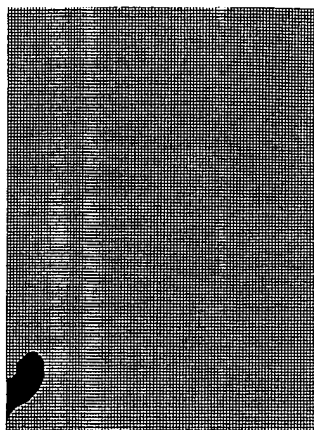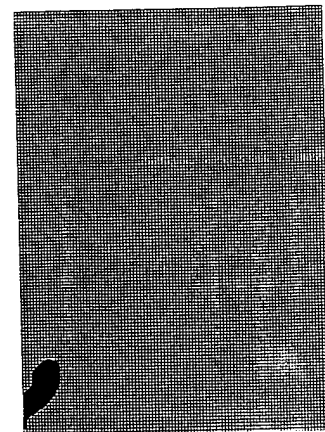Figure 31-1.   Bubble Shape for Flat Rigid Boundary Case with h* = 1.16

(a) at Time = 0.95T   (b) at Time = 0.98T
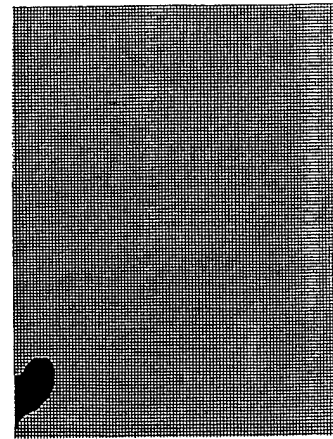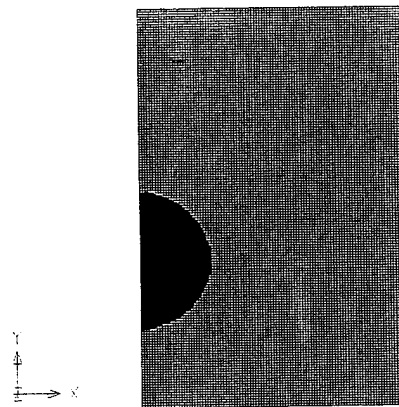

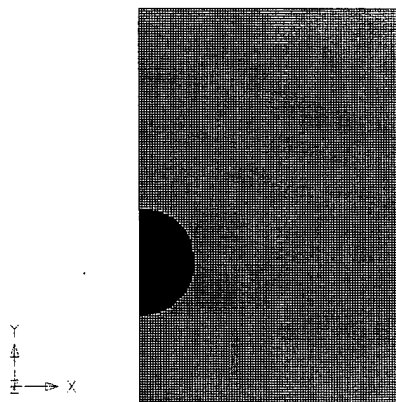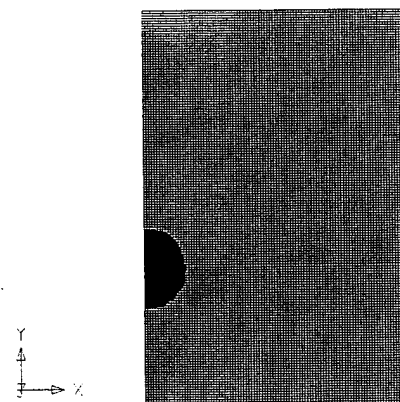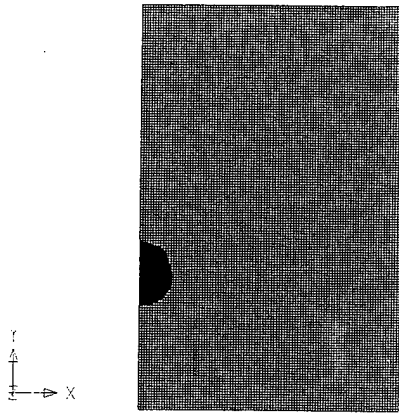(c) at Time = 0.99T   (d) at Time = 1.00T

Figure 31-2.   Bubble Shape for Flat Rigid Boundary Case with h* = 1.16
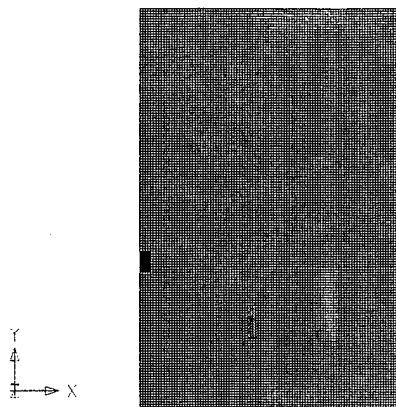
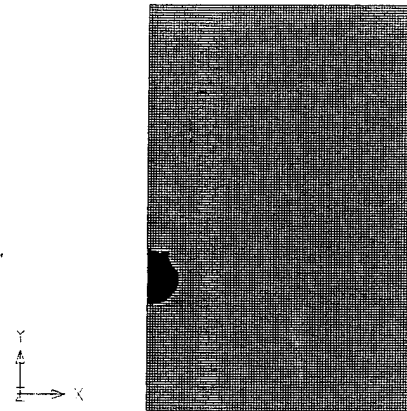(a) at Time = 0.0T

(b) at Time = 0.50T

(c) at Time = 0.80T

(d) at Time = 0.90T
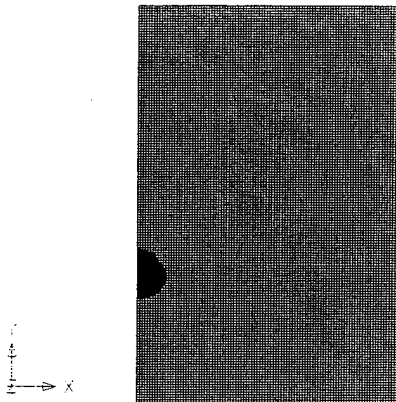
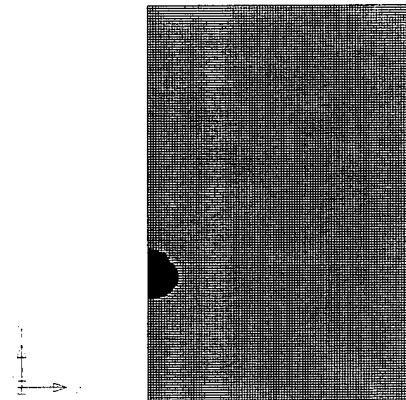Figure 32-1. Bubble Shape for Flat Rigid Boundary Case with h* = 2
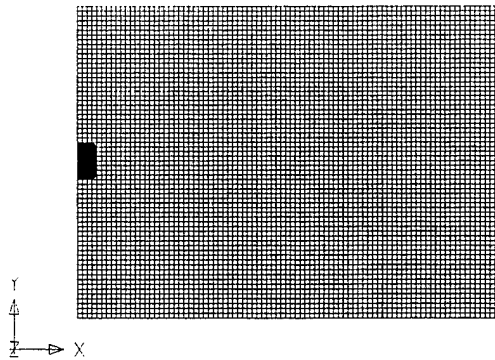
(a) at Time = 0.95T
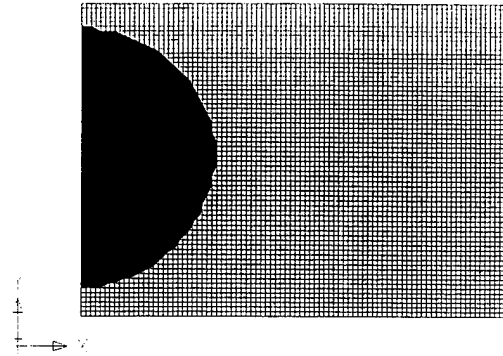

(b) at Time = 0.98T
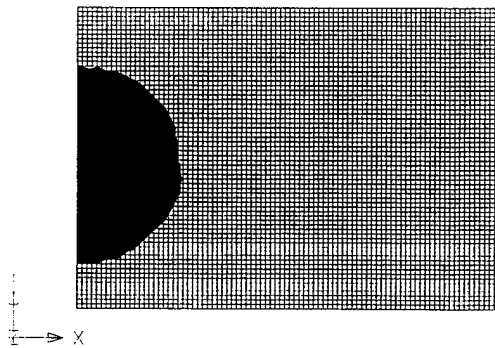

(c) at Time = 0.99T

(d) at Time = 1.00T

Figure 32-2.   Bubble Shape for Flat Rigid Boundary Case with h* = 2
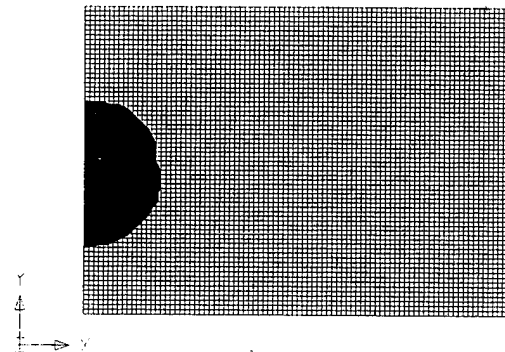
(a) at Time = 0.0T

(b) at Time = 0.50T
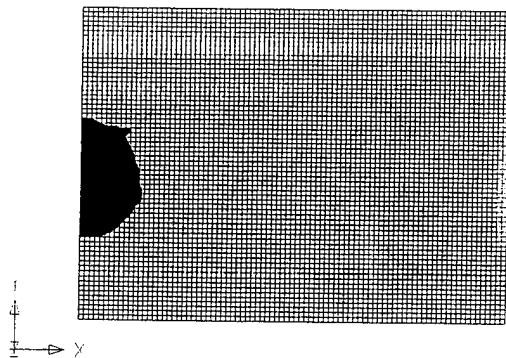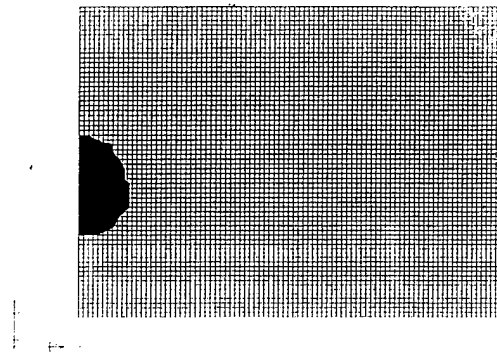
(c) at Time = 0.80T

(d) at Time = 0.90T
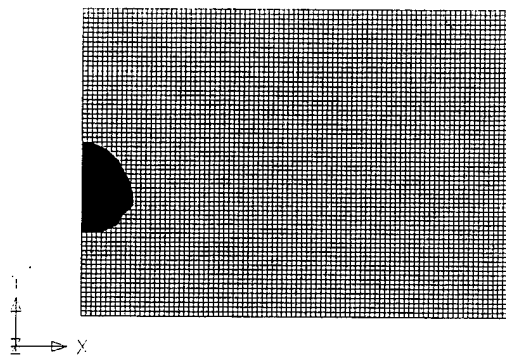
Figure 33-1.   Bubble Shape for Rigid Boundary Case

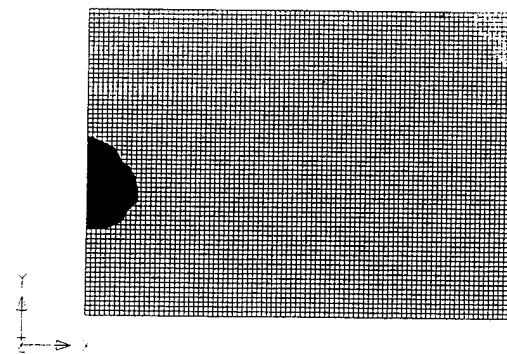for Positive Curvature with r* = 10 and h* = 2

(a) at Time = 0.95T

(b) at Time = 0.98T

(c) at Time = 0.99T

(d) at Time = 1.00T

Figure 33-2.   Bubble Shape for Rigid Boundary Case

for Positive Curvature with r* = 10 and h* = 2

LIST OF REFERENCES

1   COLE, R. H., *Underwater Explosion*, Princeton University Press, Princeton, NJ, 1948.

2   Chisum,J.E. and Shin,Y.S., Multimaterial Eulerian and Coupled Lagrangian-Eulerian Finite Element Analysis of Underwater Shock Problems, Report NPS-ME-95-001, Naval Postgraduate School, Monterey, CA, 1995.

3   *MSC/DYTRAN Users Manual: MSC/DYTRAN Version 2.2*, The MacNeal Schwendler Corporation, Los Angeles, 1994.

4   Dobratz, B. M., *LLNL Explosives Handbook*, UCRL-52997, Lawrence Livermore National Laboratory, Livermore, CA, 1981.

5   Shin, Y.S. and Geers, T. L., Response of Marine Structures to Underwater Explosion (class notes), February, 1993.

INITIAL DISTRIBUTION LIST

No. of Copies

1. Defense Technical Information Center 2
    8725 John J. Kingman Rd., STE 0944
    Ft. Belvoir, VA 22060-6218

2. Dudley Knox Library 2
    Naval Postgraduate School
    411 Dyer Rd.
    Monterey, CA 93943-5002

3. Professor Young S. Shin, Code ME/Sg 1
    Department of Mechanical Engineering
    Naval Postgraduate School
    Monterey, CA 93943-5002

4. Department Chairman, Code ME 1
    Department of Mechanical Engineering
    Naval Postgraduate School
    Monterey, CA 93943-5002

5. Naval Engineering Curricular Office (Code 34) 1
    Department of Mechanical Engineering
    Naval Postgraduate School
    Monterey, CA 93943-5002

6. LCDR James E. Chisum 1
    Department of Mechanical Engineering
    Naval Postgraduate School
    Monterey, CA 93943-5002

7. LT. Matumoto. Kazuhiro 1
    1st Engineering Section
    1st Engineering Division
    Engineering Department
    Defense Agency Maritime Staff Office
    Tokyo, Minato-ku, Akasaka, 9 - 7 - 45
    Japan